Science Requirements Document

for the

Constrained Vapor Bubble (CVB) Experiment

Peter C. Wayner, Jr.[†] and Joel L. Plawsky
Department of Chemical Engineering
Rensselaer Polytechnic Institute
Troy, New York 12180-3590

April 27, 2001

revision G
February 27, 2009

[†]Tel: (508) 276–6199; Fax: (518) 276–4030; email: wayner@rpi.edu

Signature Page for Microgravity Science Division
Science Requirements Document

Title of Experiment: **Constrained Vapor Bubble (CVB)**

Date: February 27, 2009

SRD Version: April 27, 2001 – revision G

Peter C. Wayner, Jr. Principal Investigator Rensselaer Polytechnic Inst. Troy, NY 12180-3590	Date	Joel L. Plawsky Co-Investigator Rensselaer Polytechnic Inst. Troy, NY 12180-3590	Date

Concurrance

NASA Glenn Research Center

David F. Chao Project Scientist	Signature	Date
Ronald J. Sicker Project Manager	Signature	Date
Fred J. Kohl ISS Research Program Manager	Signature	Date

NASA Headquarters Approval

Francis P. Chiaramonte ISS Research Project Program Executive	Signature	Date

Signature Page for Microgravity Science Division
Science Requirements Document
ADDENDUM - July 28, 2004

Title of Experiment: **Constrained Vapor Bubble (CVB)**

Date: February 27, 2009

SRD Version: April 27, 2001 – revision G

Peter C. Wayner, Jr. Principal Investigator Rensselaer Polytechnic Inst. Troy, NY 12180-3590	Date	Joel L. Plawsky Co-Investigator Rensselaer Polytechnic Inst. Troy, NY 12180-3590	Date

Concurrance

NASA Glenn Research Center

David F. Chao Project Scientist	Signature	Date
Ronald J. Sicker Project Manager	Signature	Date
Fred J. Kohl ISS Research Program Manager	Signature	Date

NASA Headquarters Approval

Francis P. Chiaramonte ISS Research Project Program Executive	Signature	Date

Revisions:

SRD Version: April 27, 2001

Revision A – April 27, 2001

- newly dated version of SRD updated from February 6, 2001, rev. G version
- incorporated comments and corrections from Pete's fax dated 4-25-01
- incorporated comments and corrections from Mike's email dated 4-26-01
- edited §5.7 Test Matrix and Experiment Operations
- edited §5.8 Success Criteria
- edited §5.9 Post-Flight Deliverable to the Principal Investigator
- created success criteria summary table (Table 3)
- removed ~~strikeout~~ and insert markups
- spellchecked

Revision B – April 28 – May 3, 2001

- per email from Pete dated May 1, 2001:
  - removed *vapor* from step 2 of §5.7.1
  - included *heat input and heat rejection to cooler* in step 1 of §5.9
- per telephone conversation with Pete on May 3, 2001:
  - changing operating temperature range from 20–40 °C to 15–35 °C to insure that the internal pressure of the test cell remains below 1 atm.
- corrected various typos

Revision C – October 28, 2002 – October 31, 2002

- removed spurious 1 from first paragraph of §5
- revised the requirement for the minimum volume of liquid in the test section in §5.4.1
- revised temperature accuracies in §5.4.3 to ±0.5%
- updated experimental verification in §5.4.4
- revised accuracy requirement for "tracking temperature" to ±0.5 °C in §5.5.2
- revised curvature measurements (§5.6.1) so that the maximum curvature is 20,000 m^{-1}
- heat input/rejection accuracy changed to ±10% (§5.6.4)
- updated temperature measurement requirements (§5.6.5)
- modified test matrix narrative (§5.7) to reflect changes in curvature measurements
- updated CVB test matrix summary table
- updated dry cell and wet cell operations (§5.7.1 & §5.7.2)

Revision D – March 28, 2003

- removed ~~strikeout~~ and insert markups of Revision C
- updated §5.1; science requirements summary table

Revision E – July 28, 2004

- added addendum to signature page for new project scientist and new headquarters authorization for SRD updates and corrections
- corrected grammatical error in Table 1, §5.3
- eliminated experimental validation from §5.4.4
- provided upper heater temperature limit for dry test cell heat input requirements (§5.5.1)
- added temperature range for liquid-vapor fill ratio (§5.4.1)
- added note to §5.4.3 regarding the pressure transducer during isothermality checks
- updated description of "tracking temperature" location in §5.5.2 to better reflect the current CVB test cell configuration
- updated telepresence requirement (§5.5.3)
- clarified rationale for sampling rate in §5.6.1, §5.6.2 and §5.6.3
- included "debris" with small bubbles in description of flow disruption in §5.6.3

Revision F – July 29, 2004

- removed ~~strikeout~~ and insert markups of Revision E
- corrected spelling error in §5.6.3
- removed "For the dry test cell, the heater temperature need not exceed 400 °C." from §5.5.1. This requirement was added in Revision E but is unnecessary because of the temperature limit specified in the operations requirement of §5.7.1.

Revision G – April 15, 2008

- updated test matrix in §5.7
- updated wet cell operations in §5.7.2
- updated minimum success criteria in §5.8.1
- updated ground test requirement in §4.3
- updeted that current models will be used in §4.6

Contents

Abstract

The thermophysical principles underlying change-of-phase heat transfer systems controlled by interfacial phenomena under microgravity conditions are not well understood. As a result, related passive engineering systems have not been optimized. Herein, we propose basic experimental and theoretical studies of the nonisothermal constrained vapor bubble (CVB) under microgravity conditions to help remedy this undesirable situation. This proposed study is multi-faceted: 1) it is a basic scientific study in interfacial phenomena, microgravity fluid physics and thermodynamics; 2) it is a basic study in thermal transport; and 3) it is a study of a passive heat exchanger. Although the basic scientific Facets (1) and (2) are initially emphasized, the research naturally leads to the development of a passive heat exchanger optimized for microgravity conditions.

The proposed optical study of a vapor bubble constrained in a transparent glass cell under nonisothermal conditions will increase the basic understanding of transport systems controlled by interfacial phenomena. The pressure gradient field will be obtained optically whereas the temperature field will be obtained using thermal sensors. Due to the sensitivity of systems of the proposed relatively large size to gravity and to small temperature and pressure gradients, these transport systems need to be studied under microgravitational conditions. An "axisymmetric" system with a small Bond number is required. Direct extensions to the microgravity environment of current earth based studies (which are described in Appendices A, B, & C) are proposed. The augmented Young-Laplace equation and the Kelvin-Clapeyron model will be used. Background information on the general Kelvin-Clapeyron model is given in Appendix (D).

The immediate macroscopic objectives are to determine the stability, the fluid flow characteristics, the average heat transfer coefficient in the evaporator, and the heat conductance of the CVB as a function of the heat flow rate and vapor volume. The immediate microscopic objective is to determine the detail characteristics of the transport processes in the curved liquid film. The local conditions under which cavitation and instability occur with the formation of a dry region will be determined as a function of heat flux, film thickness and stress. High fluxes and relatively large systems with small capillary pressures will be emphasized. Both completely wetting (Pentane) and partially wetting (Ethanol) fluids will be studied and compared.

1 Introduction

1.1 Motivation

The use of interfacial free energy gradients to control fluid flow naturally leads to simpler and lighter heat transfer systems because of the absence of mechanical pumps. Therefore, "passive" engineering systems based on this principle are ideal candidates for the space program. In this context, "passive" refers to the natural pressure field for fluid flow due to changes in the intermolecular force field under an imposed nonisothermal temperature field. This force field is a function of the shape, temperature, and composition of the system. For example, heat pipes which rely on these forces have been proposed frequently to optimize heat transfer under microgravity conditions. However, the basic thermophysical principles controlling these systems are not well understood and, as a result, they have under performed. In general, the full potential of interfacial forces has not been realized in transport phenomena. **Herein, we propose basic experimental and theoretical studies of the constrained vapor bubble (CVB) under microgravity conditions to help remedy this undesirable situation.** The proposed use of a transparent glass cell and related optical measurements will increase the understanding of transport systems controlled by interfacial phenomena because the system is viewed directly. Relatively large systems with high heat fluxes and small capillary pressure levels set in the condenser will be emphasized.

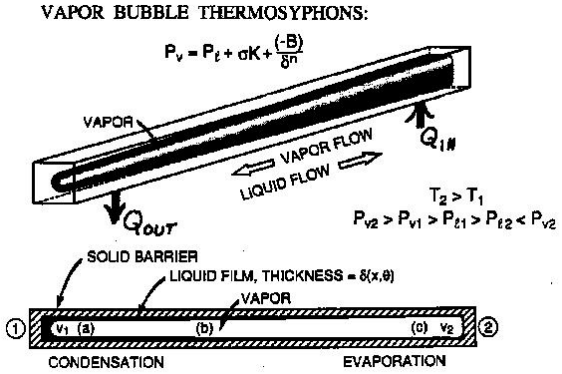

Figure 1. Constrained Vapor Bubble (assumptions: $B < 0$ for wetting system and $g \to 0$)

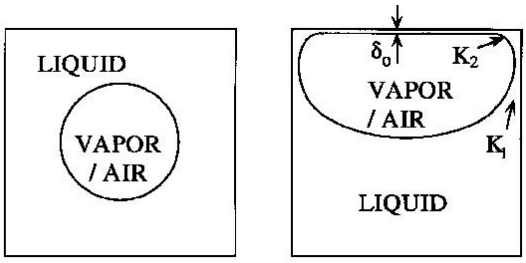

Figure 2. Exaggerated schematic comparison of cross-sections of microgravity and ground-based liquid film profiles. $K_1 < K_2$.

In particular, we are concerned with the experimental study of the CVB presented in Figure 1. For a completely wetting system, the liquid will coat all the walls of the chamber. On the other hand, for a finite contact angle system, some of the walls will have only a small amount of adsorbed vapor which changes the surface properties of the solid-vapor interface. Liquid will fill at least a portion of the corners in both cases. If temperature $T_2 > T_1$ because of an external heat source and sink, energy flows from End (2) to End (1) by conduction in the walls and by an evaporation, vapor flow and condensation mechanism. The condensate flows from End (1) to End (2) because of the intermolecular force field which is a function of the film profile. There is a "pressure jump" at the

liquid-vapor interface, $P_l - P_v$, due to the anisotropic stress tensor near interfaces. The evaporation and condensation regions are connected by an intermediate region which can be approximately isothermal and adiabatic if the system is operated so that $Q_{out} = Q_{in}$.

This proposed study is multi-faceted: 1) it is a basic scientific study in interfacial phenomena, fluid physics and thermodynamics; 2) it is a basic study in thermal transport; and 3) it is a study of a passive heat exchanger for use in microgravity. Facet (3) will have the lowest priority when conflicts concerning direction arise. The research is synergistic in that the proposed CVB research requires a microgravity environment and the space program needs thermal control systems like the CVB. We propose that relatively large systems (millimeter compared to micro) and small pressure gradients (on average) are needed for both optimum performance and convenient experimental study. However, these large systems are easily distorted by the earth's gravitational field. Due to the sensitivity of systems of this size to gravity and to small temperature and pressure gradients, these thermal control systems need to be studied under the microgravitational conditions of intended use. "Axisymmetric" systems with small Bond numbers are required. The term axisymmetric is used herein to mean reflective symmetry with respect to the length axis of the CVB.

The proposed research is based on our current theoretical and earth based experimental programs. Results from current equilibrium and non-equilibrium studies are presented in Appendices (A-D) which are an integral part of this Science Requirements Document (SRD). **Direct extensions of these earth based studies to the microgravity environment are proposed.**

1.2 Scientific Objective and Significance

When the gravitational body force is essentially removed, the shape of a constrained liquid-vapor volume with a free interface changes dramatically to reflect the new force field. Schematics of the system are presented in Figures 1 & 2. The resulting isothermal equilibrium shape depends on the gravitational field and the intermolecular force field which changes rapidly in the vicinity of the liquid-vapor and liquid-solid interfaces. This equilibrium liquid film shape in a particular gravitational field is controlled by fixing the container shape, the liquid-substrate system, and the relative volume of the liquid to that of the vapor. We propose that the extended Young-Laplace equation (Equation 1, Appendix A and Equation 10 below) describes this shape over a large range of conditions. The validity of this model has been experimentally demonstrated in our laboratory (DasGupta et al., 1995, Appendix A).

Under non-equilibrium conditions resulting from an imposed temperature gradient, fluid flow and change-of-phase heat transfer are a function of further changes in the shape of the liquid volume. We propose that the shape dependent interfacial intermolecular force field passively controls fluid flow and heat transfer, and that these non-equilibrium effects can be analyzed using a Kelvin-Clapeyron transport model (e.g., see DasGupta et al., 1993a & b, 1994, Appendix D). This model includes the use of the conservation of heat, mass and momentum and the extended Young-Laplace equation. To date, this transport model has been studied only under normal gravitational conditions which limits the range of experimental conditions (e.g., heat flux, liquid to vapor volume ratio and the

size of the system) that can be effectively studied. In essence, an asymmetric gravitational field complicates the details of the transport processes. **Therefore, we propose that the Kelvin-Clapeyron transport model and system stability be evaluated experimentally using the CVB under microgravity conditions.**

On a macroscopic scale, the performance of the CVB heat exchanger can be evaluated by measuring heat in and heat out along with the axial variation of the temperature and liquid film profiles in the CVB as a function of the vapor volume. These measurements will be made with and without liquid in the cell for comparison. The value of the parallel conductance in the glass walls will be subtracted from the overall conductance to obtain the conductance due to the processes of evaporation, vapor flow, condensation and return liquid flow. Changes in the wall temperature profile will indicate these processes. In addition, measurement of the meniscus profile in the intermediate section will give the pressure gradient for condensate flow. This will allow the calculation of a heat balance. Simple visual inspection through the microscope will indicate the overall bubble shape and location which are needed to verify the interpretation of the temperature profile. **The immediate macroscopic objectives are to determine the overall stability, the fluid flow characteristics, the average heat transfer coefficient in the evaporator, and heat conductance of the CVB as a function of vapor volume and heat flow rate.** These heat transfer measurements constitute an innovative and useful but relatively simple heat transfer study. In our current laboratory experiments, the liquid flow rate in the upper corners is different from that in the bottom corners because of different liquid profiles in the fillets due to gravity. The nonisothermal pressure gradient for liquid flow in the corners is proportional to the curvature raised to the fourth power. Therefore, the heat transfer process in the upper region of the cell can be significantly different from that in the bottom under 1 g conditions. Under microgravity conditions, the evaluation of additional heat losses along the outer surface of the CVB will also be simplified because asymmetric losses due to natural convection will be absent. In our current laboratory studies, the relative size of these asymmetric losses, which limits the choice of experimental conditions and cause Marangoni flow, are a function of the temperature level of the study.

On the microscopic scale, the scientific objective is to evaluate the local details of the Kelvin-Clapeyron model of change-of-phase heat transfer under microgravity conditions where the extended Young-Laplace equation predominates. This will lead to a fuller understanding of stability and transport processes controlled by interfacial forces under microgravity conditions.

Axisymmetric systems (defined on page 2) are required for detail studies concerning the Kelvin-Clapeyron transport model. Herein, we will discuss these nonequilibrium studies in conjunction with microscopic and macroscopic procedures. Another long term engineering objective, which is not an explicit part of this basic scientific study, is to use these results to design heat transport systems uniquely suited to microgravity conditions.

For the purpose of an overall perspective, a brief description of an evaporating partially wetting liquid film will be given at this point. As the axial heat flow rate increases in the CVB presented in Figure 1, a portion of the hot end dries out due to viscous losses in the recirculating fluid. A qualitative schematic of the dry area on one of the walls is presented in Figure 3. The junction of

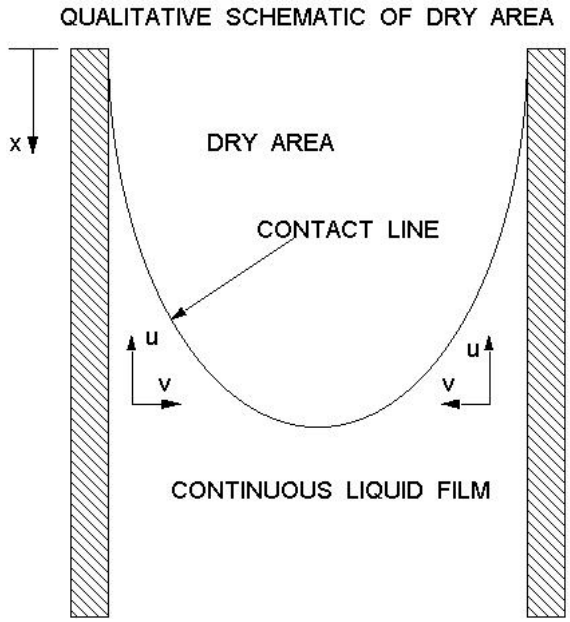

Figure 3. Qualitative schematic of the junction of the dry and wet regions on one of the walls of the CVB.

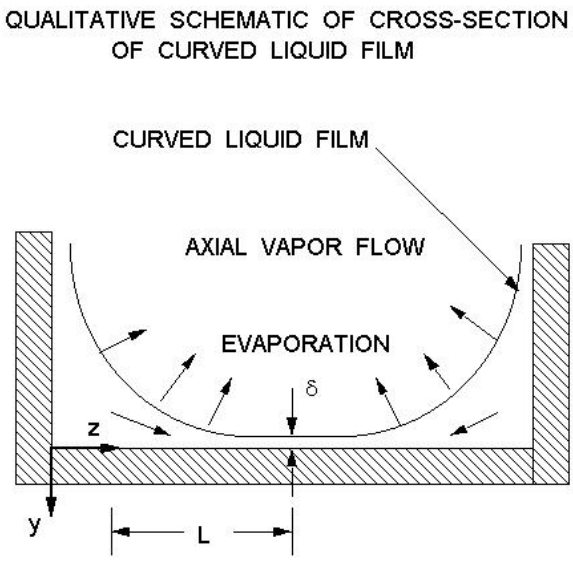

Figure 4. Qualitative schematic of the cross-section of the continuous film region in the evaporator section.

the dry area and the liquid film is the contact line. A qualitative schematic of the cross-section of the continuous film region is given in Figure 4. Fluid flows mainly in the relatively large corner fillets in the axial "x" direction from the condenser and then in the curved thin film region across the walls of the CVB where evaporation occurs. At a particular heat flux which is a function of the overall size of the system, the local film thickness and stress, a dry area forms. One microscopic objective of the proposed research is to evaluate the details of this evaporation/dryout phenomenon. A related macroscopic objective is to determine the general stability of the system and the shape of the dry region.

1.3 Justification for Extended Microgravity Environment

In addition to the asymmetric natural convection losses and asymmetric fillet areas mentioned above, other factors also effect the choice of system size and experimental conditions. We propose that both axisymmetric and relatively large ***average*** liquid film thicknesses are needed to optimize heat transport because viscous losses are minimized in thick films. These conditions cannot be achieved in a 1 g environment. A microgravity environment allows a greater latitude in the selection of the liquid/vapor volume ratio and the total vapor volume that can be accurately studied. This can be appreciated partially by comparing the liquid-vapor interfacial profiles presented in Figure 2. The asymmetric shape in the earth's gravitational field, which represents an asymmetric pressure field, is much more difficult to control, use and analyze. The effect of interfacial forces on the transport processes is uncontrollable in small capillary pressure systems in the earth's gravitational field

because of the relative size of the gravitational force field. On the other hand, thicker liquid films will give larger liquid flow rates and, therefore, heat transfer rates. In addition, axisymmetric systems are needed to evaluate the details of the Kelvin-Clapeyron transport model. Since steady state conditions are required for the experiments, ground-based reduced-gravity facilities are inadequate because transient changes associated with transport phenomena damp out slowly.

In general, the physical principles associated with the shape and stability of the liquid volume in a CVB need to be evaluated and modeled under steady state microgravity conditions. An analytical justification is presented below in Section 3.

1.4 Large and Small Scales

The CVB presented in Figure 1 has both large and small scale characteristics. Throughout the system under microgravitational conditions, fluid flows as a result of the intermolecular forces of liquid-liquid cohesion and liquid-solid adhesion. This pressure field for flow results from an imposed external temperature field which causes a nonuniform liquid film to form due to evaporation/condensation. The pressure field is revealed and obtained by measuring the shape of the liquid volume. The pressure field and resulting transport processes can be studied at the molecular, microscopic and macroscopic levels.

At the junction of the liquid film with the vapor and the solid substrate (which can have a nonevaporating adsorbed film), the liquid film thickness can be (but does not need to be) the thickness of a monolayer. This junction has been called the contact line or interline which is of general importance to the field of wetting with or without transport. The exact details of the contact line region are extremely complicated and depend on whether the fluid is a completely wetting fluid or a partially wetting fluid on the experimental substrate.

The contact line thickness is controlled by the imposed experimental conditions. A monolayer thickness can be obtained by imposing a large superheat at the contact line. At the other extreme of the proposed experimental temperature (heat flux) design, the thinner part of the evaporating liquid film can have a thickness of approximately 0.25 μm. At the other end of the nonisothermal CVB where condensation occurs, the thickness of the liquid film can be much larger (approximately, 1.5 mm). Therefore, depending on the experimental conditions, extremely large variations in the thickness scale within the CVB are possible. Under some nonisothermal conditions, the heat flux in the contact line region can be enormous. On the other hand, the flux can be substantially less a short distance away where the film thickness is much larger. Therefore, we find in this deceptively simple device an enormous range in both the scale and the level of transport processes. For example, under equilibrium conditions, it is a thermodynamic cell in which interfacial properties can be accurately studied. Under nonequilibrium conditions, a very dynamic transport system can be studied. The fundamental question is "How can this system be optimized for use as a passive heat exchanger under microgravity conditions?"

We can study the following broad categories in the CVB: 1) Effect of intermolecular forces,

temperature and liquid/vapor volume ratio on the isothermal equilibrium liquid film thickness profile; 2) Effect of intermolecular forces, liquid/vapor volume ratio and temperature on the average phase change transport processes over a relatively large area (i.e., the overall macroscopic heat flow rate, average fluid flow rate, average heat transfer coefficient, and stability); and 3) Effect of intermolecular forces, liquid/vapor volume ratio and temperature on phase change over a very small area (i.e., the local heat flux distribution, local fluid flow rate, and stability). These areas of research can be further subdivided with the adjectives transient and steady state. Herein, we propose steady state (and natural oscillatory) studies within Categories (2 & 3). First, the stability and average value of the transport processes occurring over a large area, Category (2), will be emphasized. Axial fluid flow due to capillarity in the intermediate region will be measured. The size of the dry area will be determined as a function of axial heat flow rate and vapor volume. The value of the thermal conductance and average heat transfer coefficient will be determined. Then, Category (3), the details of the transport processes in the contact line region, which is always present and important, will be emphasized. Category (3) calculations will be made using the data obtained during the initial flight. Sufficient Category (1) studies have already been made in our laboratory to justify the use of the extended Young-Laplace equation.

1.5 Literature Review

For many years, the classical Young-Laplace equation of capillarity has been successfully used to describe the pressure jump due to the anisotropic stress tensor at a curved liquid-vapor interface under equilibrium conditions (see e.g., Concus, 1968). Examples of its use to describe nonequilibrium fluid dynamics in micro heat pipes and grooves are given in publications by Ha and Peterson (1998), Wu and Peterson (1991) and by Khrustalev and Faghri (1993). In these cases, the pressure jump causing fluid flow is a function of the liquid-vapor surface tension and the interfacial radius of curvature. However, near the liquid-solid interface, additional changes in the stress field within the liquid occur because of changes in the intermolecular force field due to solid molecules replacing liquid molecules. This leads to the extended Young-Laplace model, which includes both capillarity and long range van der Waals forces, for the pressure jump at the liquid-vapor interface (Derjaguin and Kussakov, 1939, Dzyaloshinskii et al., 1961, Derjaguin et al., 1965, Huh and Scriven, 1971, Potash and Wayner, 1972, Blake, 1975, Derjaguin and Churaev, 1976, Teletzke et al., 1976, Renk et al., 1978, Kamotani, 1978, Holm and Goplen, 1979, Moosman and Homsy, 1980, de Gennes, 1985, Truong and Wayner, 1987, Wong et al., 1992, DasGupta et al., 1991, 1993 a&b, 1994, 1995). These long range van der Waals forces have been found to be extremely important in that they lead to the concept of an extended evaporating meniscus and the Kelvin-Clapeyron model (see e.g., Potash and Wayner, 1972, Wayner et al., 1976, Kamotani, 1978, Wayner, 1979, DasGupta et al., 1991, 1993a&b, & 1994, Appendix B, Stephan and Busse, 1992). In a completely wetting evaporating system, a thin adsorbed film extends for a long distance beyond the classical equilibrium meniscus (e.g., Derjaguin et al., 1965, Wayner, 1991). The thin film controls the important processes of spreading and wetting. It forms a thin liquid bridge between the "classical menisci" formed in the corners of the chamber presented in Figures 1 and 2. On the other hand, some experimental results have been presented that question the validity of the augmented Young-Laplace equation: Using aqueous films, Lam and Schechter (1991) found deviations from the predicted profile obtained us-

ing a technique presented by Hirasaki (1990). One possible reason for this inconsistency is the use by Lam and Schechter of highly polar water which is affected by additional forces in a thin film. One objective of the research proposed herein is to investigate the validity and consequences of the extended meniscus phenomena using nonpolar fluids in a heat transport system akin to the micro heat pipe. **We note that the proposed study is generic with uses beyond those associated with a heat pipe.** Nevertheless, it is useful to relate the current system to a micro heat pipe in the next paragraph because of the cell shape being used in the proposed study.

Many papers have been published on the modeling of micro heat pipes since Cotter's original paper (1984). For example, Peterson (1992) and Faghri (1995) have written excellent reviews of micro heat pipe research and development that include both experimental investigations on micro heat pipes and modeling of micro heat pipe performance. Recently, Khrustalev and Faghri (1993) and Swanson and Peterson (1993) have used models based on the augmented Young-Laplace equation to analyze a micro heat pipe. Heat transfer from a stable evaporating thin film in the neighborhood of a contact line was analyzed by Brown et al., (1993). Swanson and Herdt (1992) have used the three dimensional augmented Young-Laplace equation to develop a mathematical model describing the details of the evaporating meniscus in a capillary tube. Babin et al. (1990) present a steady state model that assumes prior knowledge of the liquid film profile in order to compute the liquid and vapor pressure drops. Longtin et al. (1994) have also developed a one-dimensional model to predict the operating parameters of the micro heat pipe. Their analysis differs from ours mainly in the boundary conditions. Also, the factor they use to compare their model results to experiments is the macroscopic heat flux instead of a more fundamental parameter (the film curvature profile) which we propose to use herein. The optical measurement of the curvature profile is unique to our studies.

Therefore, we can conclude that there is sufficient previous research done under normal gravitational conditions using very small dimensions to warrant microgravity studies. The proposed use of microgravity will extend the experimental dimensions and conditions that can be accurately studied. Larger systems with smaller capillary pressures can be studied in microgravity. In addition, the use of a transparent glass cell with related optical profile measurements will give additional insights based on visual observations.

2 Proposed Translation of Current Ground Based Studies to a Microgravity Environment

2.1 Equilibrium studies (see Appendix A for details)

The isothermal profiles of the extended meniscus in a quartz cuvette were measured in the earth's gravitational field using an image analyzing interferometer (IAI) which is based on computer enhanced video microscopy of the naturally occurring interference fringes. These profiles are a function of the stress field. Experimentally, we found that the extended Young-Laplace Equation is an excellent model for the force field near the solid-liquid and liquid-vapor interfaces for heptane and pentane menisci on quartz and tetradecane on SFL6. The effects of refractive indices of the solid and the liquid on the measurement techniques were demonstrated. The experimentally obtained values of the disjoining pressure and the dispersion constants were compared to those predicted from the DLP (Dzyaloshinskii-Lifshitz-Pitaevskii, 1961) theory for an ideal surface and reasonable agreements were obtained. A parameter was introduced that gave a quantitative measurement of the closeness of the system to equilibrium. The nonequilibrium behavior of this parameter was also presented.

Since we predict that these earth based results concerning the extended Young-Laplace Equation would be confirmed under microgravity conditions, microgravity equilibrium studies are not proposed. However, equilibrium studies will be done in the earth's environment using the newly designed NASA cell to avoid surprises.

2.2 Nonequilibrium Macroscopic Studies of the "Adiabatic" Intermediate Section (see Appendix B for details)

A nonisothermal constrained vapor bubble heat exchanger, CVB, was modeled and experimentally studied in the earth's gravitational field. Using a relatively simple pentane/quartz system, the fundamental parameters governing the CVB (namely, temperature, pressure, and menisci curvature profiles) were measured. An intermediate "adiabatic" section wherein the temperature remained nearly constant was identified. This intermediate section was kept relatively adiabatic with regard to natural convection losses by keeping the temperature level in the cell close to that in the surroundings. A one-dimensional steady state model of this "adiabatic" section of the CVB was developed and solved numerically to yield pressure, velocity, and film curvature as a function of the axial position. Using Image Analyzing Interferometry, IAI, the experimentally obtained curvature profiles agreed very well with those predicted by a macroscopic one-dimensional friction factor model. An equation for the curvature is given in Section 4.7. The operating temperature of the "adiabatic" region was found to be a function of the operating pressure which could be controlled by the thermoelectric coolers located in the condensation section. The performance of the heat exchanger was evaluated by measuring heat in along with the temperature and liquid film

thickness profiles in the CVB. The system was found to be very sensitive to both internal and external conditions. Due to the gravitational field, undesirable asymmetric flow fields were present. Therefore, the details of the Kelvin-Clapeyron transport model and stability were not evaluated.

Expanded studies under microgravity conditions are proposed. The primary difference between our ground based macroscopic studies and the proposed microgravity studies is the lack of symmetry in the 1g fluid flow areas when gravitational field is not parallel to the CVB axis. Therefore, the heat fluxes were asymmetric. Although desirable from a fluid transport point of view, relatively large values of the liquid flow area cannot be properly controlled in the earth's gravitational field. In addition, the axisymmetric flow fields in microgravity will allow the evaluation of the details of the Kelvin-Clapeyron transport model with an accurate evaluation of stability (plus oscillations and cavitation).

2.3 Nonequilibrium Macroscopic Studies of the Evaporator Section (see Appendix C for details)

A two dimensional equation for the temperature distribution in the evaporator section of the CVB was presented by Huang et al. (1998). An area averaged heat transfer coefficient was used to account for the complicated heat transfer mode on the inside wall of the cell. In essence, the model allows the unknown heat transfer coefficient to be obtained from the measured temperature profile. We propose to use the techniques presented in Appendix C along with macroscopic video pictures of the axisymmetric dry and wet areas to obtain the average heat transfer coefficient in the evaporator and an understanding of stability.

2.4 Microscopic Nonequilibrium Studies of the Evaporation and/or Condensation Sections Using the Kelvin-Clapeyron Model

We also propose to extend the above macroscopic study of the CVB to a microscopic basic study in thermal sciences using the microscopic profile of the liquid in the CVB to obtain local values of the evaporation rates and an understanding of the effect of instabilities. The objective of this portion of the proposed research is to evaluate the use of a Kelvin-Clapeyron type model of change-of-phase heat transfer under conditions in which the augmented Young-Laplace equation predominates. Important detailed information concerning contact line motion, instabilities and cavitation will be obtained. Numerical modeling is also envisioned. Again, the advantage of a microgravity environment is that the cross-section of the liquid profile will be symmetric around the axis of the CVB over a broad range of conditions.

General background information concerning the Kelvin-Clapeyron model is given in Appendix D. Please note that the cell design used in this background paper is not the design proposed for the flight tests. The model would have to be adjusted for the axisymmetric CVB cell design. In

addition, we do not propose to use the ellipsometer in the flight experiments. This would be a good extension of the experiments in the future.

2.5 Steady State and Stability Behavior of Partially Wetting Working Fluids

The experimental use of a second fluid, which would be partially wetting, ensures the observation of instabilities and provides comparisons with results obtained using the completely wetting fluid, pentane. The use of ethanol as a partially wetting second fluid would enhance the observations and measurements associated with contact line instabilities, boiling and dryout. We tested ethanol as a potential partially wetting candidate and found that it does act sufficiently different to warrant its inclusion as a second fluid. With ethanol, a boiling phenomena can be observed near the contact line, which has a finite contact angle and a dry region, and the contact line oscillates more readily than with pentane. In addition, a region of dropwise condensation, which is indicative of a partially wetting fluid, can be observed at low heat fluxes. This region of dropwise condensation and the easy propensity to boil were not observed with pentane.

We note that the results using ethanol were obtained using a vertical cell which gives an axisymmetric system (defined on page 2). Therefore, a complete numerical comparison with our previous results cannot be made at this time because the axial pressure gradient in the vertical cell is affected by the earth's gravitational field, which is not the case with the previously used horizontal cell. The disadvantage of the horizontal cell is that the system is asymmetric. Experiments to determine the numerical details of the differences using the vertical cell with pentane are planned for the year 2000.

3 Justification for Extended Microgravity Environment

3.1 Justification for Relatively Large Liquid/Vapor Volume Ratios

In general, heat pipes use wicks with very small pores to optimize their control and performance. In conventional micro heat pipes, the amount of liquid is relatively small with control and symmetry resulting from the small radius of curvature and thinness of the liquid film. However, for the proposed CVB heat exchanger experiments, relatively large axisymmetric dimensions are desirable for both optimum performance and experimental reasons. To demonstrate this we start with the following macroscopic analysis for a completely wetting one-dimensional curved film.

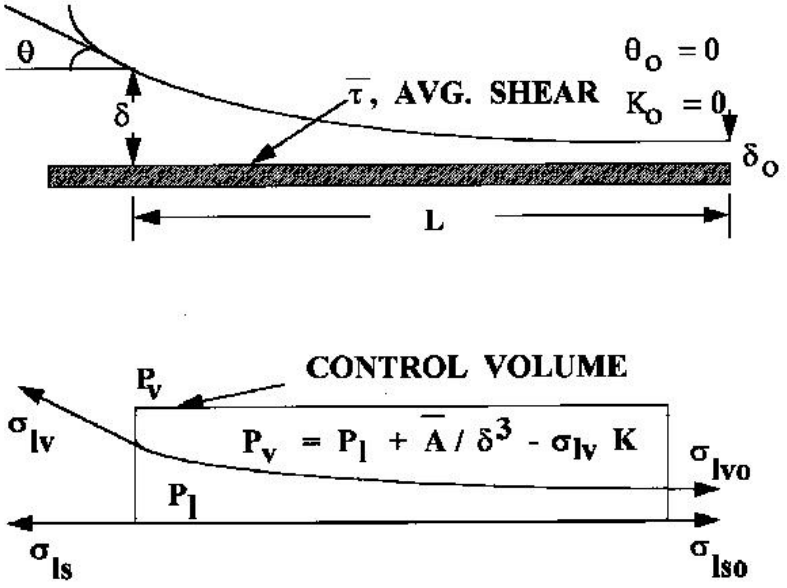

Figure 5. Control volume for macroscopic horizontal force balance due to interfacial free energy.

A macroscopic horizontal force balance (per unit width) for the completely wetting ($\bar{A} < 0$), nonpolar, meniscus presented in Figure 5 gives Equation (1) (Kim and Wayner, 1996).

$$\sigma_{lv}\cos\theta + \sigma_{ls} + \sigma_{lv}\mathrm{K}\delta + \frac{-\bar{A}}{\delta^2} + \bar{\tau}L = \sigma_{lvo} + \sigma_{lso} + \sigma_{lvo}\mathrm{K}_o\delta_o + \frac{-\bar{A}}{\delta_o^2} \tag{1}$$

Background for the interfacial forces that led to this result can be found in papers by deFeijter (1988), Martynov, et al. (1977), and Wayner (1991). Equation (1) can be simplified to Equation (2)

using the following assumptions: $\sigma_{ls} = \sigma_{lso}$, $\sigma_{lv} = \sigma_{lvo}$, $\mathrm{K}_o = 0$, in which the subscript "o" refers to the location of the interline, δ_o. The first two assumptions restricts the contact line thickness to approximately $\delta_o > 1$ nm and the third assumes that the substrate is smooth.

$$\sigma_{lv}(1 - \cos\theta) = \bar{\tau}L + \sigma_{lv}\mathrm{K}\delta + \frac{\bar{A}}{\delta_o^2} - \frac{\bar{A}}{\delta^2} \tag{2}$$

We find that the apparent contact angle, θ, at the thicker end is a function of the viscous losses and interfacial forces. Taking this end to be the condensing end of the vapor bubble in the CVB, we can assume that $\theta = 90^\circ$, and $\delta \gg \delta_o$. In addition, the curvature at this location approaches a constant value if the thickness, δ, is sufficiently large so that the local viscous stresses are relatively minor. Using these assumptions to simplify the above, gives

$$\bar{\tau}L \approx \sigma_{lv}(1 - \mathrm{K}\delta) - \frac{\bar{A}}{\delta_o^2} \tag{3}$$

As an approximation, $\mathrm{K}\delta \to 1$ at the condensing end of the vapor bubble in the CVB and Equation (3) becomes

$$\bar{\tau}L \approx -\frac{\bar{A}}{\delta_o^2} \tag{4}$$

This demonstrates that the viscous losses in the *completely wetting* film are approximately equal to the "suction" due to interfacial van der Waals forces at the contact line. The average shear stress is proportional to the average velocity, $\bar{V}$ and inversely proportional to the average film thickness, $\bar{\delta}$:

$$\bar{\tau} \sim \frac{\mu\bar{V}}{\bar{\delta}} \tag{5}$$

Therefore,

$$\bar{V} \sim -\frac{\bar{A}\bar{\delta}}{\mu\mathrm{L}\delta_o^2} \tag{6}$$

For the internal area, aH, given in Figure 2, an order of magnitude estimate of the average one-dimensional axial heat flux is

$$q'' \sim \frac{2\bar{V}\bar{\delta}(a+H)\rho_l h_{fg}}{aH} \tag{7}$$

We note that, since the average film thickness is an unknown, Equation (7) is useful only for the discussion of trends. Additional modeling is presented below in Section 4.7. Using Equations (6 and 7) and $a = H$ for a square cross-section, the following proportional equation is obtained for the axial heat flux:

$$q'' \sim \left(\frac{-Ah_{fg}}{\nu}\right)\left(\frac{4}{\delta_o^2}\right)\left(\frac{\bar{\delta}H}{H^2}\right)\left(\frac{\bar{\delta}}{L}\right) \tag{8}$$

The first group on the right-hand side is an interline heat flow rate parameter and is a function of the physical properties of the system. For the pentane/glass system it has a value of approximately 10^{-9} watts at room temperature. The second group represents the suction at the contact line which is inversely proportionally to the square of the thickness at the contact line. We note that,

although this term gives a feel for the phenomena, it does not describe the complicated irregular details or stability at the contact line. The third group represents the ratio of the average area for fluid flow to the overall internal area which we use as an effective area for heat flux. (Conduction in the walls of the CVB is not included.) The last group represents the relative effect of the average film thickness to that of the length of the shear stress area on the heat flux.

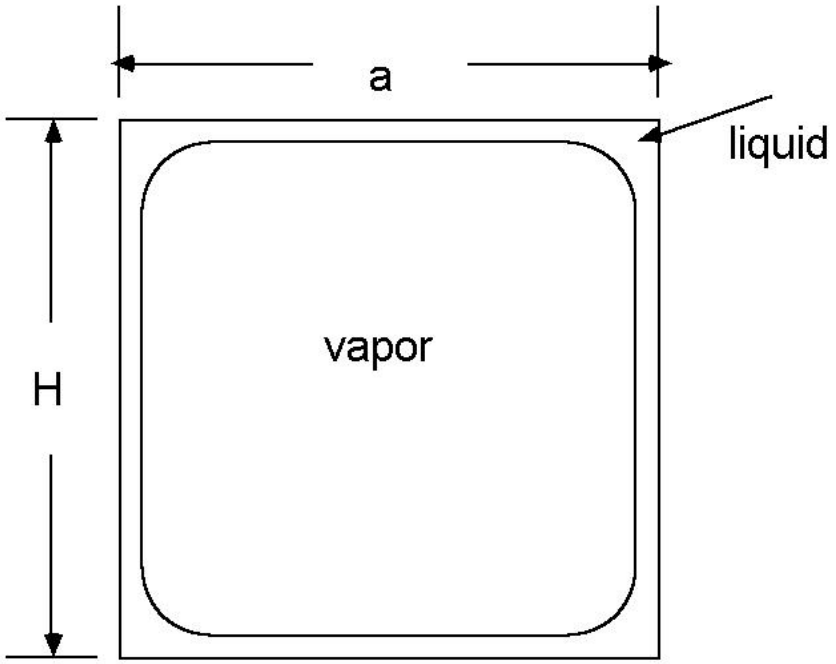

Figure 6. Cross-section of inside of CVB.

Rewriting Equation (8) using a dimensionless average film thickness $\Delta = \bar{\delta}/\sqrt{HL}$, gives

$$q'' \sim 4\left(\frac{-Ah_{fg}}{\nu\delta_o^2}\right)\Delta^2 \tag{9}$$

The average film thickness, $\bar{\delta}$, increases with H if we keep the vapor volume constant. Although we do not know the details of this function, we predict that the heat flux increases with average liquid film thickness and, therefore, H because of the reduction of viscous losses. On the other hand, the upper limit of the axial heat flux is restricted also by the maximum stable value of the heat flux in the contact line region. We note that Longtin, et al. (1994) predicted the same effect of the system size on heat flux. How well this can be achieved in large systems can be determined experimentally only in microgravity because relatively large symmetric systems cannot be studied in the earth's gravitational field. In addition, larger systems with the proposed dimensions are easier to study optically because of the separation between adjacent fringes viewed with the IAI. For the purpose of experimental design, an equation for the predicted curvature profile in the proposed CVB cell as a function of heat flow rate is given below in Section 4.7.

3.2 Theoretical Justification for Microgravity Environment

Although relatively large CVB systems with small viscous losses and small interfacial forces outside the interline region are desirable from a heat flux perspective, the same reductions in viscous losses and interfacial forces make the system susceptible to acceleration and gravity. Historically, these effects are discussed in terms of the Bond number, Bo, which is discussed next. The extended Young-Laplace Equation for the equilibrium system presented in Figure 2 is

$$\sigma \mathrm{K} + \Pi + (\rho_v - \rho_l) g z = 0 \tag{10}$$

Using a reference capillary pressure, $\sigma \mathrm{K}_\infty$, gives

$$\frac{\mathrm{K}}{\mathrm{K}_\infty} + \frac{\Pi}{\sigma \mathrm{K}_\infty} - \frac{(\rho_l - \rho_v) g z}{\sigma \mathrm{K}_\infty} = 0 \tag{11}$$

The third group is a local Bond number. For $z = H$ and $\mathrm{K}_\infty \approx 2/H$ the relative effect of gravity and system size is obtained:

$$\mathrm{Bo} \approx \frac{\rho_l - \rho_v) g H^2}{2\sigma} \tag{12}$$

To obtain a symmetric system we need $\mathrm{Bo} \to 0$. For a typical alkane,

$$\mathrm{Bo} \approx 2.3 \times 10^4 g H^2 \tag{13}$$

For our proposed microgravity study with $g = g_\mu$, and the characteristic width of the microgravity experimental cell, $H_\mu = 3 \times 10^{-3}$, Equation (13) gives

$$\mathrm{Bo} \approx 0.21 g_\mu \tag{14}$$

Therefore, a microgravity environment allows us to obtain our goal of both a symmetric system and low stress field. To obtain the same symmetry on the earth, a much smaller value of H is needed:

$$H = \sqrt{\frac{g_\mu}{g}} H_\mu \tag{15}$$

However, the stress field is inversely proportional to the system size, H. Therefore, we find that the twin objectives of symmetry and a low stress field can only be achieved in a microgravity environment. We note that, to evaluate the macroscopic thermal conductance in much smaller systems, micro heat pipes systems are currently being studied in the earth's environment using nontransparent walls (see, e.g., Peterson, et al., 1992). We note that the use of high thermal conductivity nontransparent metal walls does not allow the required optical measurements.

A qualitative understanding of the effect of system size on the thickness of the adsorbed thin film can be obtained using Equation (10) with $g \to 0$. We note that Equation (10) represents an isothermal equilibrium system. In this case, we find the following relationship between the film thickness, δ, and system size, H:

$$\delta = \left(\frac{-\bar{A}}{\sigma \mathrm{K}} \right)^{1/3} \cong \left(\frac{-\bar{A} H}{2\sigma} \right)^{1/3} \tag{16}$$

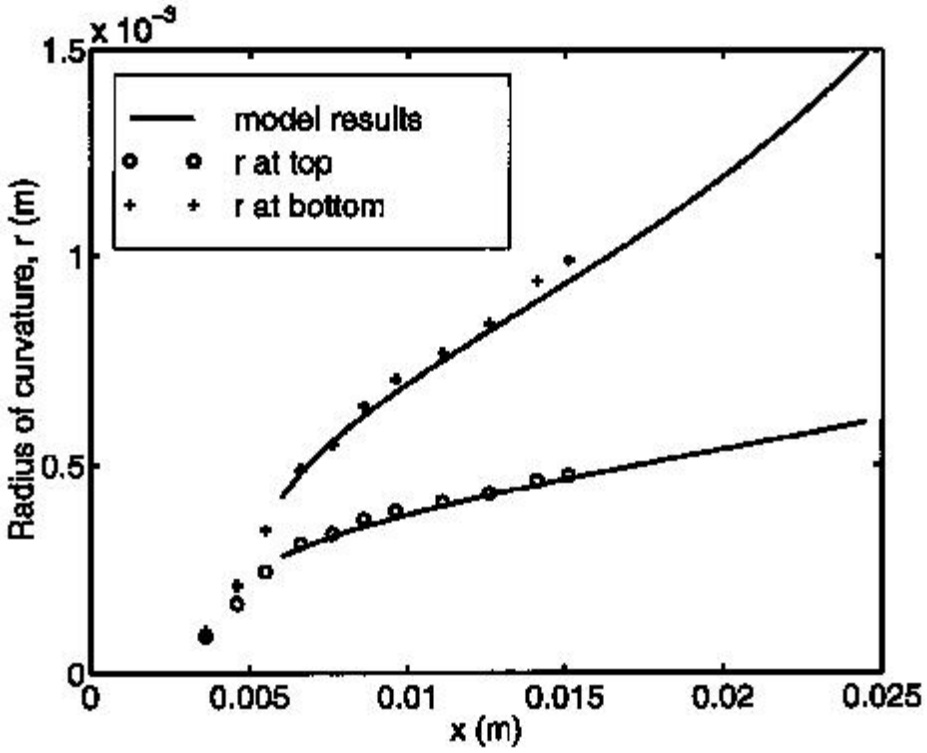

Figure 7. Variation of experimental top radius of curvature with axial position and comparison with r at bottom.

Therefore, an increase in the width of the system, which gives a larger radius of curvature at the colder end, leads to a thicker flat thin film between the fillets.

3.3 Justification for Microgravity Environment (Experimental Observations)

For the relatively low heat flux experimental results discussed in Appendix (B1), the inclination angle of the cell was $\theta = 0°$. More recent results in (B2) using various inclination angles demonstrated that the effect of gravity on the heat transfer process in the CVB is substantial at some heat fluxes. We found that the heat transfer process at the top of the cell was different from that at the bottom of the cell. For example, at high heat fluxes, an asymmetric boiling process at the hot end was observed with a horizontal cell whereas an asymmetric dryout zone at the hot end was observed with a cell inclined at an angle of $\theta = 10°$. In addition, more fluid flowed in the fillets on the bottom of the cell than in the fillets at the top. Some of this additional fluid probably flowed from the bottom to the top of the cell in the fillets at the hot end. Therefore, as expected, the heat transfer process was found to be a complicated function of the angle of inclination and the angle of rotation in a gravitational field.

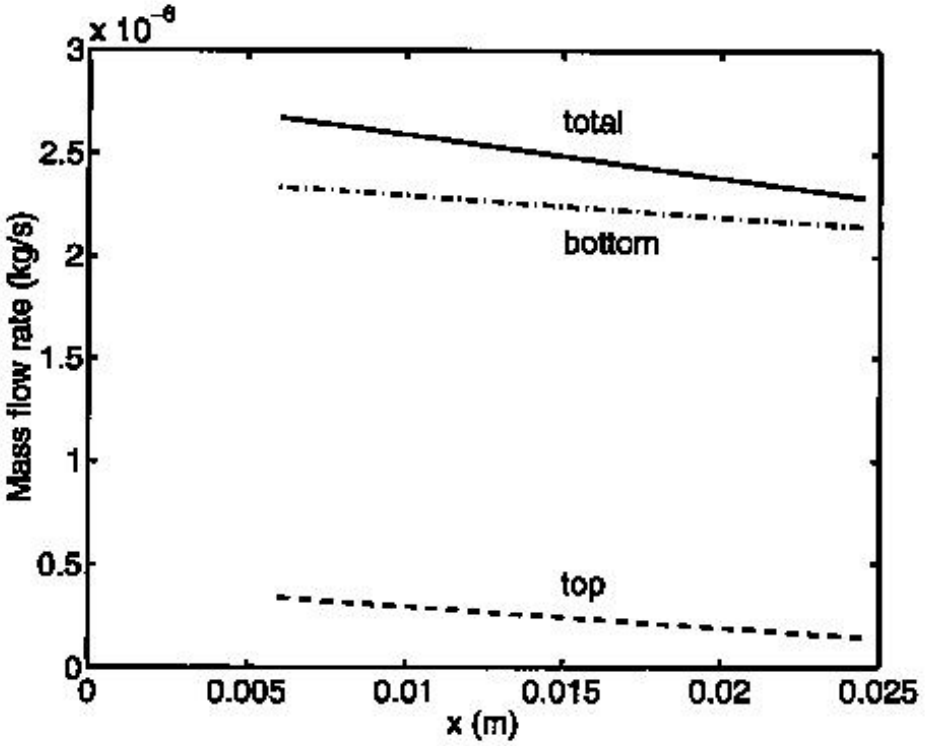

Figure 8. Comparison of mass flow rates in the top and bottom fillets.

As an example of the asymmetry of the system at 1g , we present some recent results in Figures 7 & 8. The procedures discussed in Appendix B were used except that the angle of inclination of the cell was $\theta = 4.35°$. In Figure 7, the measured value of the radius of curvature in the top corner of the cell is presented as a function of the axial position. The theoretical value of the radius of curvature profile at the bottom of the cell is also presented. The corresponding values of the calculated flow rates due to capillarity in the top and bottom of the cell are presented in Figure 8. In addition the heat fluxes are a function of the angle of rotation because of the natural convective currents around the cell and the variation in the thickness of the liquid film with the angle of rotation. Therefore, at some heat fluxes at 1g, boiling would occur at the bottom of the cell and thin film evaporation would occur at the top of the cell with possible turbulent flows between the bottom and top. All these differences preclude the accurate use of the one-dimensional Kelvin-Clapeyron transport model to evaluate experimental data in the CVB in the earth's environment. A microgravity environment is required to simplify the process by making it axisymmetric.

3.4 Justification for Extended Microgravity Environment

In general, transient transport processes are associated with relatively long time scales. For example, if the liquid-vapor interface in an isothermal CVB was studied using an airborne low-gravity

facility, the interface would still be evolving after the short flight time. Takamatsu et al. (1996) have presented experimental results for an air-liquid mixture in a small cylindrical pipe installed in a free fall capsule in a drop shaft facility. The glass pipes used in their experiments had a length of 150 mm and inside diameters of 5, 7, and 9 mm. They found that the air-liquid system formed a number of bubbles with liquid plugs with nearly equal spacing. However, we feel that the final configuration for the constrained system observed after 10 seconds was probably unstable because the persistence of constrained liquid plugs seems unreasonable from the perspective of minimum interfacial free energy. The proposed microgravity tests would experimentally test this hypothesis under both isothermal and non-isothermal conditions. We note that we could not produce more than a single bubble by shaking our smaller square cell (3 x 3 mm) in our laboratory. The maximum stable and desirable cross-sectional area is an unknown. We also note that, in our current experiments under normal gravitational conditions, thermal changes take hours to reach steady state.

4 Experimental Flight Plan

4.1 Rationale

The objective of the proposed flight experiment is the experimental study of a relatively large CVB with relatively small pressure gradients under microgravity conditions where the system will be symmetric with respect to the axis. Symmetric systems with small interfacial pressure jumps (large radii of curvature) cannot be obtained in the earth's gravitational field. Due to the sensitivity of the system to small pressure and temperature gradients and gravity, these thermal control systems should be studied under microgravitational conditions. The studies of the overall dynamics of the CVB will increase our basic understanding of interfacial phenomena and aid the design of future microgravity cooling systems. The operating conditions presented below will include tests in which the stability limits of the evaporating thin film to high heat fluxes will be explored.

By using a relatively large liquid/vapor volume ratio, relatively large heat fluxes with large axial pressure gradients will be studied. By using a set of liquid/vapor volume ratios, a systematic evaluation of the effect of liquid shear stress on the evaporative heat flux will be obtained. For example, with a very short vapor bubble, the corners at the hot end of the cell will always be supplied with liquid. Whereas, with a relatively long vapor bubble, the corners of the cell near the hot end will dry out at high heat fluxes. Since the base of the meniscus in the corners for these two cases have different capillary pressures, the characteristics of the extended part of the meniscus would be different. As discussed in Section 3.1, the shear stress is inversely proportional to the liquid film thickness at a given heat flux.

4.2 General Specifications

We propose to use an experimental design based on our current heat transfer studies, which are presented in Appendices (B & C). In essence, we are proposing that the techniques developed and tested in our laboratory be optimized for use in a microgravity environment. To minimize and simplify the payload, the CVB will be charged with liquid and sealed before launch.

The dominant design considerations are : 1) cell cleanliness and fluid purity; 2) a symmetric steady state test environment; 3) accurate control of both the heat input and heat output; 4) accurate measurements of the liquid film thickness and temperature profiles, and the vapor pressure; and 5) optimum light level and alignment with the optical microscope which are essential for sharp interference fringes. A set of small cuvettes will be evacuated and then filled with the working fluid on earth before launch. Each cuvette represents a particular liquid/vapor volume ratio which will be tested individually. The details of the "science requirements" for measurements and accuracy are presented below in Section 5.

4.3 Sequential Test Plan

Phase I: Current Ground-Based Studies.

During the current ground-based experimental Phase I studies, valuable experience is being obtained. The initial results are presented in the appendices. However, additional modeling, experimental study and experience are needed. Models and computer programs to evaluate the experimental data need to be developed and evaluated. An expanded range of test conditions need to be studied. For example, higher heat fluxes and the effect of these heat fluxes on the stability of the system need to be examined. Fluid purity and its effects on the transport characteristics are important additional considerations. For example, the CVB acts as a natural distillation system, with the higher boiling component migrating to the hot end. We note that the volume of the contact line region is extremely small compared to the volume of the cell. Therefore, very small concentrations (< 0.1 %) of a second similar component can be tolerated but larger concentrations cannot. Large values of impurities, like those discussed in Appendix (C), will *not* be used. There is a possibility that an extremely small amount of a second component will enhance the stability of the system in the contact line region. Finally, the shape of the CVB cell needs to be optimized to insure the correct stable location of a single vapor bubble.

Ground based experimental studies using the CVB cell in and outside the NASA vacuum chamber to determine the three dimensional temperature distribution in the walls of the CVB are recommended. These can be numerical and/or experimental based on using an IR camera. Numerically, the one dimensional axial temperature profile (measured using thermal sensors) can be expanded to three dimensions. The IR camera can be used for experimental verification. In addition, the potential use of an IR camera in the flight experiment can be evaluated.

Phase II: Build and Pre-Flight Test a New CVB Cell.

Although our current experimental cell gives good data, we find that enhanced mechanical skills are needed to optimize the final cell fabrication for the μg environment. Therefore, we propose that the co-principal investigators work with NASA personnel to design and build a working model of the flight CVB cell. The flight cell will be ground tested at Zin-Tech facilities before being sent to the ISS. Therefore the same flight cell will be operated in both the 1 g and the μg environment. Current software programs for data analyses need to be optimized. Key items that must be addressed are:

1. The subsystem that includes the CVB heat transfer cell, the heaters, the coolers, and the pressure transducer needs to be simplified and built. The individual parts must be well aligned with the optical system;
2. The filling sequence needs to be developed further to insure fluid purity, cleanliness, and an accurate liquid/vapor volume ratio. Procedures and designs to insure the proper location of the vapor bubble must be developed and evaluated;
3. An optical system needs to be developed that allows the individual cuvettes to be placed with proper alignment for the flight experiments. Efficient programs to determine the film

thickness and curvature profiles need to be further optimized.

4. Accurate temperature measurement and heat flux evaluation schemes need to be developed.
5. The radiative characteristics of the system need to be evaluated.
6. Automated experimental sequences need to be developed.

Phase III: Flight.

The final construction and assembly of the Microgravity CVB Test Equipment will be performed by NASA. Using a similar cell, studies to determine the Hamaker constant and radiative characteristics will be done at Zin-Tech. The details of the flight experiments are given in the following sections.

4.4 Experimental Detail

Except for improved control, extended experimental requirements (e.g., liquid/vapor volume ratio), improved optical equipment design, temperature measurement techniques with thermal mapping (3 dimensional temperature profiles), and testing under microgravity conditions, the experiments will generally follow those currently being developed in our laboratories like those reported in Appendices (A, B & C). Additional details on data acquisition and modeling follow.

4.5 Data Acquisition

The seven most important quantities that must be measured are:

1. The film thickness profile using the IAI (Image Analyzing Interferometer described in Appendices A & B);
2. The temperature profile;
3. The pressure level in the cell;
4. The power input at one end of the cell and the power output at the other end of the cell;
5. The general location of the vapor bubble (e.g., is there a second vapor bubble, and whether or not there is some liquid accumulated at the hot end due to a distillation effect);
6. The shape of the dry area, oscillations, cavitation and instabilities if present; and
7. Before launch, the Hamaker constant, the radiative characteristics, the liquid/vapor volume ratio and the purity in the CVB.

These measurements will be used as described in Appendices (A, B, C & D).

4.6 Mathematical Models

The CVB will be modeled using the following levels of complexity:

1. Under equilibrium conditions before launch using a comparable cell, the meniscus profile will be used to evaluate the extended Young-Laplace equation as discussed in Appendix A. In essence, the Hamaker constant will be experimentally determined and compared with the DLP model;
2. Under non-equilibrium conditions on a macroscopic scale, the overall heat flow rate and effective thermal conductance in the CVB will be obtained from the model and the measured values of the temperature profile, heat input and output as described in Appendix B;
3. Under non-equilibrium conditions on a macroscopic scale, the average heat transfer coefficient in the evaporator section of the CVB will be obtained from the model and the measured values of the temperature profile, heat input and output as described in Appendix C;
4. Under non-equilibrium conditions on a macroscopic scale, the overall stability of the film in the CVB will be observed as a function of heat flow rate and vapor volume. The size of the dry area on the wall will be obtained The presence of oscillations and cavitation will be evaluated.
5. Under non-equilibrium conditions on the macroscopic scale, the pressure gradient in the intermediate region will be obtained from the model and optical measurement of the meniscus profile as described in Appendix B. See additional material in Section 4.7 below;
6. Using (3 -5) above, a macroscopic heat balance that equates liquid flow rate and heat flow rate will be obtained;
7. Under non-equilibrium conditions on the microscopic scale, the two-dimensional meniscus profile will be used with the Kelvin-Clapeyron model as described by DasGupta et al. (1994) to obtain the local rates of evaporation and condensation in their respective regions. Two and three dimensional numerical thermal modeling will be used if necessary to evaluate and confirm the Kelvin-Clapeyron model of fluid flow and evaporation based on the film profile; and
8. Under non-equilibrium conditions on the microscopic scale, a stability analysis based on the experimental observations will be made (we anticipate that, at some currently unknown values of the heat flow rate, oscillations will start and migration of the contact line to form a dry area will occur).

During our initial flight experiment, we propose to emphasize Parts (2-6) listed above. Since data will be available, Parts (7 & 8) will be addressed in at least a preliminary manner. In all cases the improved models described in our annual reports will be used.

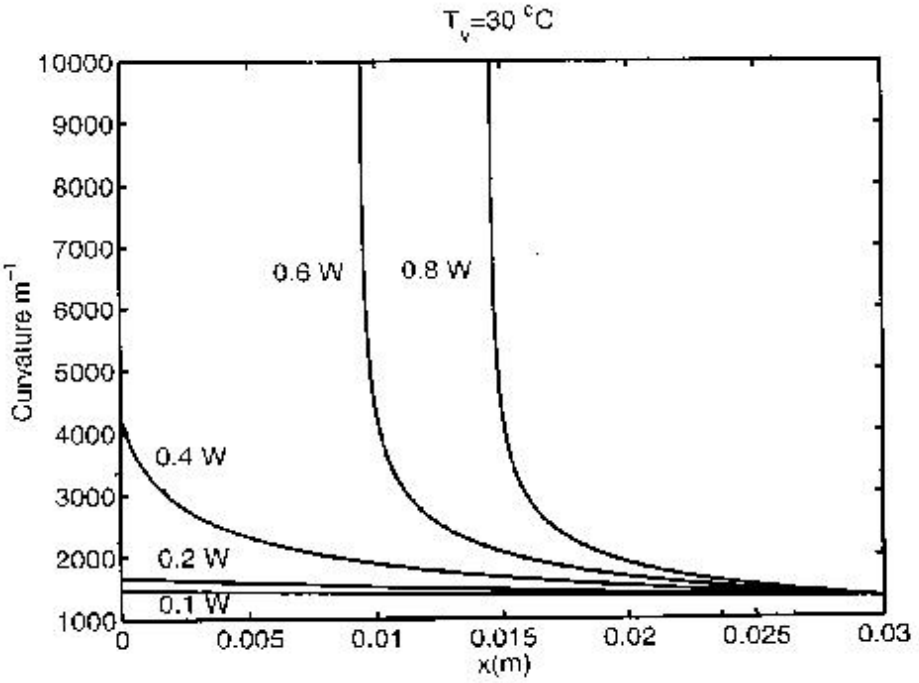

Figure 9. Theoretical value of the curvature in the corners versus axial position for various values of the axial heat flow rate.

4.7 Theoretical axial profile of the corner curvature

In Figure 9, the theoretical value of the curvature in the corners of the CVB is plotted as a function of the axial position and the axial heat flow rate, Q. The values were obtained using Equation (17), which is based on a balance between the viscous losses due to liquid flow in the corner and the capillary pressure gradient.

$$\frac{1}{\mathrm{K}^3} = \frac{1}{\mathrm{K}_c^3} - \frac{3\nu k_{fl} Q}{C_L^3 \sigma h_{fg}}(L - x) \tag{17}$$

We find that, depending on the value of the axial heat flow rate, the corners dryout ($\mathrm{K} \Rightarrow \infty$) at a particular axial position. Since this is based on a one-dimensional model of axial liquid flow in the corners, the result is only approximate. The effect of a two dimensional flow pattern needs to be experimentally determined and modeled. On the other hand, the one dimensional model gives a conservative basis for the design of the experimental equipment. The two dimensional curvature gradient would be lower since additional area would be available for liquid flow in the extended menisci.

4.8 Application of the Results

The studies outlined above represent the first axisymmetric, micro-gravity test of the concepts discussed in Appendices A -D. The characteristics of the non-isothermal thickness profile will be evaluated as a function of the heat flow rate and the liquid/vapor volume ratio. The characteristics of the transport processes will be determined as a function of the liquid/vapor volume ratio and heat flow rate. The stability of the non-isothermal thickness profile will be evaluated as a function of the heat flow rate, the local capillary pressure level, and the liquid/vapor volume ratio. The Kelvin-Clapeyron transport model will be evaluated. The results obtained using a completely wetting fluid (e.g., Pentane) will be compared with those obtained using a partially wetting fluid (e.g., Ethanol). Subsequent to these basic microgravity studies, the results will be used to obtain heat transfer correlations for the design heat exchangers for use in a microgravity environment.

5 Science Requirements

In this section, the science requirements, the test matrix, the experiment operations, and the success criteria are described. A summary table of the science requirements is presented first with a narrative of each requirement presented in subsequent sections. The requirements for the test fluid and the test cell are given in §5.2 and §5.3, respectively. The environmental conditions which must be met prior to and during experiment operation are specified in §5.4. The control requirements for the CVB experiment are given §5.5 and §5.6 defines the required accuracy, range, etc. of the experiment measurements. Following the specification of the science requirements, the test matrix, experiment operations and success criteria, §5.7 to §5.8, are defined. Finally, the post-flight deliverables to the principal investigator are specified in §5.9.

5.1 Science Requirements Summary Table

Table 1: Summary of Science Requirements

Parameter	**Section**	**Experiment Requirements**
Fluid and Fluid Purity	§5.2	
working fluid		Pentane Ethanol
liquid purity		$>$ 99.9 %, see narrative in §5.2
vapor purity		$\leq$ 5 torr non-condensables
Test Cell & Test Cell Cleanliness	§5.3	
cell geometry		parallelepiped with radius of all interior corners $<$ 1 μm.
cell dimensions		square cross section with inside dimensions of 3 $\times$ 3 mm $\pm$ 2%. test cell length sufficient to accommodate liquid-vapor fill ratio, see §5.4.1

Table 1: Summary of Science Requirements

Parameter	**Section**	**Experiment Requirements**
wall thickness		1.25 mm ± 2%.
test cell material		standard quartz (fused silica) for UV-Vis spectrophotometry
test cell cleanliness		see narrative in §5.3
§5.4 Experiment Setup & Environment Requirements		
Liquid-Vapor Fill Ratio	§5.4.1	prior to experiment operation:
vapor volume – Pentane Cell 1		bubble length of 20 mm ±5% at 20 °C ± 2 °C
Pentane Cell 2		bubble length of 30 mm ±5% at 20 °C ± 2 °C
Pentane Cell 3		bubble length of 40 mm ±5% at 20 °C ± 2 °C
Ethanol Cell 1		bubble length of 25 mm ±5% at 20 °C ± 2 °C *
Dry Cell 1		evacuated to 5 torr
minimum liquid volume		ratio of liquid-to-vapor in test section ≥ 25% liquid ± 5% at 20 °C
maximum liquid volume		vapor volume remains within ±5% over temperature range specified in §5.4.3
Liquid-Vapor Configuration	§5.4.2	prior to experiment operation: Vapor exists as a single bubble located between the evaporator and the condenser.
Thermal Environment	§5.4.3	prior to experiment operation:
nominal temperature		between 15 °C and 35 °C

*The size of the bubble and putity of the ethanol is being reevaluated

Table 1: Summary of Science Requirements

Parameter	**Section**	**Experiment Requirements**
axial temperature gradient radial temperature gradient Acceleration Environment dc g-level g-jitter	§5.4.4	±0.5 °C over length of test section ±0.5 °C from side to side for 4 sides prior to and during experiment operations: Bo $< 10^{-4}$ for all dc accelerations see narrative in §5.4.4
Other Environment Req.	§5.4.5	There are no known nor anticipated requirements for acoustic, electromagnetic, or radiation environments. See narrative in §5.4.5 for requirements on humidity levels
§5.5 Experiment Control Requirements		
Heat Input Pentane test cells Ethanol test cell dry test cell uniformity	§5.5.1	 0 – 2 W ±0.5% with increments as in §5.7 0 – 2 W ±0.5% with increments as in §5.7 0 – 2 W ±0.5% with increments as in §5.7 sequence specified in test matrix, see Table 2. uniform heat generation with temperature symmetry on reflection not to vary more than 10% over the surface of the evaporator end of the test cell
Heat Rejection heat load balance	§5.5.2	 “tracking temperature” maintained between 15 & 35 °C at ±0.1 °C for 1 hr

Table 1: Summary of Science Requirements

Parameter	**Section**	**Experiment Requirements**
Telepresence	§5.5.3	for all heat inputs and ambient conditions see narrative description
§5.6 Experiment Data Requirements		
Curvature Measurements	§5.6.1	
accuracy (for pentane)		$600 \leq \mathrm{K} \leq 20,000\ \mathrm{m}^{-1} \pm 4\%$
measurement locations		locations corresponding to curvatures: $1000 < K < 4000\ \mathrm{m}^{-1}$, $\Delta K = 200$, ± 100 $4000 < K < 20,000\ \mathrm{m}^{-1}$, $\Delta K = 1000$, ± 500 measurement location relative to test cell known to within $\pm$ 0.025 mm in both lateral and axial directions
sampling rate & duration		30 Hz for at least 3 seconds
sequence of locations		time between consecutive locations $<$ 2 minutes

Table 1: Summary of Science Requirements

Parameter	**Section**	**Experiment Requirements**
Film Thickness & Adsorbed Film Measurements	§5.6.2	
range		10 nm $\rightarrow$ 20 μm
accuracy		$\pm$ 10 nm
location of film thickness measurement		center of curvature measurement location; location known to within $\pm$0.025 mm
location of adsorbed film measurement		same axial location as curvature measurement; location known to within $\pm$0.025 mm
sampling rate & duration		30 Hz for at least 3 seconds
sequence of locations		time between consecutive locations $<$ 2 minutes
Vapor Bubble Observations	§5.6.3	
field of view		length of test section
resolution		$\leq$ 500 μm
sampling rate & duration		30 Hz for duration of experiment
other		ability to detect disruption of liquid flow in corners by small bubbles with a diameter $\geq$ 100 μm
Heat Input/Rejection Measurements	§5.6.4	
accuracy		$\pm$10% for all heat inputs/rejection levels
sampling rate		1/60 Hz

Table 1: Summary of Science Requirements

Parameter	**Section**	**Experiment Requirements**
Temperature Measurements	§5.6.5	
range		-25 °C < T < 375 °C
accuracy		±0.5 °C
sampling rate		1/60 Hz
measurement locations (see Figure 11, page 39)		• test cell face for axial temp. measurement: every 1.5 mm on centerline of test section (1) at 1.5 mm from corners of condenser (1) at 1.5 mm from corners of evaporator • orthogonal face: (1) at 2mm from condenser on centerline (1) at 2mm from evaporator on centerline (1) at midpoint of test section (2) at 1.5 mm from opposite edges at midpoint • face opposite orthoganol face: (2) at 1.5 mm from opposing edges at midpoint
location accuracy		±0.25 mm; location known to within ±0.1 mm
Pressure Measurement	§5.6.6	
range		280 – 1000 Torr
accuracy		±5 Torr
resolution		±1 Torr
measurement frequency		1/60 Hz

Table 1: Summary of Science Requirements

Parameter	**Section**	**Experiment Requirements**
Acceleration Measurement	§5.6.7	
range		0 – 50 Hz, 10^{-6} to 10^{-3} g's
resolution		100 Hz, 10^{-7} g's
dc resolution		100 Hz, 10^{-5} g's
Time Correlation	§5.6.8	all data correlated to within 1/30 second

5.2 Fluid and Fluid Purity

The Science Review Panel (SRP) suggested the experimental use of a second fluid, which would be partially wetting, to both insure the observation of instabilities and for comparison with results obtained using the completely wetting fluid, pentane.

During the Summer of 1999, we tested ethanol as a potential partially wetting candidate and found that it does act sufficiently different to warrant its inclusion as a second fluid. With ethanol, a boiling phenomena can be observed near the contact line, which has a finite contact angle and a dry region, and the contact line oscillates more readily than with pentane. In addition, a region of dropwise condensation, which is indicative of a partially wetting fluid, can be observed at low heat fluxes. This region of dropwise condensation and the easy propensity to boil were not observed with pentane. We note that the results using ethanol were obtained using a vertical cell which gives an axisymmetric system. Therefore, a complete comparison with our previous results cannot be made at this time because the axial pressure gradient in the vertical cell is affected by the earth's gravitational field, which is not the case with the previously used horizontal cell. The disadvantage of the horizontal cell is that the system is asymmetric. Experiments to determine the details of the differences using the vertical cell with pentane are planned.

The use of ethanol as a partially wetting second fluid would enhance the observations and measurements associated with contact line instabilities, boiling and dryout. Significant additional data would be obtained for the comparison of the behavior of partially wetting and completely wetting fluids. Except for the upper limit on heat input/removal and the length of the CVB cell, the equipment requirements are the same for both fluids. The use of two fluids (pentane and ethanol)

is proposed.

Particulate matter, non-condensables, dissolved chemicals (i.e., normally liquids or solids at room temperature), and similar chemicals (e.g., decane versus pentane) can effect the results. Dissolved gases need to be removed by boiling the fluid before filling the cell. Dissolved chemicals are a problem because the process acts like a distillation process with the accumulation of impurities near the contact line. If the impurity has a boiling point within 15 °C of the working fluid, an impurity level of 0.1% is acceptable. However, the fluid must have no residue when it is evaporated at its normal boiling point.

Surface wetting properties of the ethanol/quartz system should be checked during assembly. In essence, when the quartz cuvette is fabricated, a high temperature is used which makes the surface slightly non-wetting to ethanol. This result should be checked during assembly to insure that it is slightly non-wetting. This process is not difficult.

5.3 Test Cell and Test Cell Cleanliness

The test cell should be a parallelepiped with radius of all interior corners < 1 μm. The test cell should have a square cross-section with inside dimensions of 3×3 mm $\pm 2\%$. The length of the test cell should be sufficient to accommodate the appropriate liquid-vapor fill ratio, see §5.4.1. The test cell material should be standard quartz (fused silica) used for UV-Vis spectrophotometry with a standard thickness of 1.25 mm $\pm 2\%$.

Particulate matter attached to the substrate in the contact line region distorts the fringe pattern. A small number of these particles can be tolerated if a clean region for fringe measurement can be located.

Each test cell should be sufficiently clean so that at least four curvature measurements at an accuracy specified in §5.6.1 can be obtained from 100×150 μm fields of view for the entire set of measurement locations.

5.4 Experiment Setup & Environment Requirements

This section describes the necessary experiment setup and environmental conditions which must be met prior to and/or during the operation of the CVB experiment.

5.4.1 Liquid-Vapor Fill Ratio

The vapor volume for each of the test cells is specified as a vapor bubble length:

Pentane Cell 1:	bubble length of 20 mm ±5% at 20 °C ± 2 °C
Pentane Cell 2:	bubble length of 30 mm ±5% at 20 °C ± 2 °C
Pentane Cell 3:	bubble length of 40 mm ±5% at 20 °C ± 2 °C
Ethanol Cell 1:	bubble length of 25 mm ±5% at 20 °C ± 2 °C †
Dry Cell 1:	evacuated to 5 torr

The minimum volume ratio of liquid to vapor **in the test section** should be at least 25% liquid, ±5% at 20 °C. In addition, liquid must be present in the corners of the test section (between the evaporator and condenser) over the entire temperature range specified in §5.4.3

These calculation should be reverified

The vapor volume should remain within ±15% over the temperature range specified in §5.4.3. This requirement on the vapor volume fluctuation determines the maximum amount of liquid in the system.

Proper liquid-vapor fill must be verified on-orbit both by a pressure measurement and by observation of the vapor bubble prior to experiment start-up.

5.4.2 Liquid-Vapor Configuration

The liquid-vapor configuration required is that of a single vapor bubble residing between evaporator and condenser. Prior to experiment start-up, the proper on-orbit liquid-vapor configuration must be verified.

The test section should have an orientation at launch to insure that the bubble migrates toward the end with the heater.

5.4.3 Thermal Environment

Prior to experiment operations, the thermal environment of the CVB test cell must be uniform and stable. The nominal temperature of the test cell must be between 15 and 35 °C. The temperature gradient along the axis of the test cell should be less than ±0.5 °C over length of test section. At any axial position along the test section, the temperature difference from side wall to side wall should be within ±0.5 °C.

Degree of isothermality should be checked by both the axial temperature data and by curvature measurements. A curvature measurement should be taken at the center of the vapor bubble ±2 mm. Two additional curvature measurements should be taken at a distance ±2 mm from the first curvature measurement. Note that prior to operation, the pressure transducer should be slightly colder than the test section. This requirement is necessary to avoid bubble migration into the transducer body due to the slight heating of the pressure transducer by the transducer electronics.

†The size of the bubble and putity of the ethanol is being reevaluated

5.4.4 Acceleration Environment

The maximum dc acceleration should not result in a Bond number greater than 10^{-4} in either the axial or radial directions relative to the CVB test cell.[‡] The Bond number is defined as

$$Bo \equiv \frac{\Delta\rho g a^2}{\sigma} \quad , \tag{18}$$

where $\Delta\rho$ is the density difference between the liquid and the vapor, g is the acceleration, a is the characteristic length scale, and σ is the surface tension. For the CVB experiment, the characteristic length scale, a, is half of the one side of the interior cross section. For example, if the test cell has a cross section of 3 mm $\times$ 3 mm, then the characteristic length scale, a, is 1.5 mm. The Bond number requirement for dc accelerations must be met over the temperature range specified in §5.4.3.

5.4.5 Other Environmental Requirements

There are no known nor anticipated requirements for the acoustical, electromagnetic, or radiation environments. Although it is undesirable to have water vapor condensing on the exterior of the test cell, no requirement on humidity will be specified. The primary concern with condensing water vapor is with the degradation of the quality of the curvature and film thickness measurements. Therefore, the humidity requirement is, by default, covered in the requirements on measurement accuracy in §5.6.1 and §5.6.2.

5.5 Experiment Control Requirements

Only two experiment parameters are actively controlled during the CVB tests; heat input and heat rejection through the cooler. The heat input is varied as part of the required test matrix. The heat rejection through the cooler is varied in order to balance the heat input and radiation losses to the surroundings.

The "Telepresence" requirements (§5.5.3) allow the principal investigator to request subsets of experiment data for verification of proper experiment environment conditions and proper experiment operation, calibration of automated algorithms, and determination of unsteady operation. The requirements for changing the operating procedure and experiment settings (heat input/rejection) are also specified.

[‡]The Bond number also specifies the maximum translational acceleration of the CVB test cell.

5.5.1 Heat Input

The range of heat inputs required for the pentane test cells and the dry test cell is 0 to 1 W. The ethanol test cell requires a heat input range of 0 to 2 W. These required heat inputs are specified as heat input into the face of the test cell. The sequence heat inputs is specified in the test matrix presented in Table 2. Summarizing the heat inputs for each test cell:

Pentane test cells	0 – 2 W ±0.5% with increments as in §5.7
Ethanol test cell	0 – 2 W ±0.5% with increments as in §5.7
dry test cell	0 – 2 W ±0.5% with increments as in §5.7

It is important that the heat input to the evaporator end of the test cell be uniform so as to insure that the capillary pumping potential in each of the four corners of the test cell is identical. Therefore, a uniform heat generation is required with temperature symmetry on reflection not to vary more than 10% over the surface of the evaporator end of the test cell. The symmetry on reflection implies the evaporator end of the test cell displays symmetry between octants.

5.5.2 Heat Rejection

The heat rejection at the condenser end of the test cell should be sufficient to maintain the "tracking temperature" between 15 °C and 35 °C at an accuracy of ±0.5 °C for a period of at least one hour. The "tracking temperature" is defined as the exterior surface temperature of the test cell at a location corresponding to the condenser meniscus. *Note that for the current configuration of the CVB test cell, the "tracking temperature" location corresponds to 1 mm towards the heater from the end of the cooler insert.* This heat rejection requirement should be met for all heat inputs. It is recommended that the "tracking temperature" be measured with a thermistor-type device and not a thermocouple.

For all heat inputs, the ratio of heat rejected by radiation to that rejected through the condenser is not a factor in the operation of the CVB experiment.

5.5.3 Telepresence

During the course of a CVB test, it may be necessary to verify proper experiment operation, calibration of film thickness and/or curvature measurements, steady or unsteady operation, etc. To that end, the principal investigator will require the ability to request downlink of a limited amount of experiment data as well as the ability to initiate changes in the conduct or operational sequence of the experiment. In addition, downlink of macroscopic views of the CVB test cell and 100×150 μm field of view images of the fringe patterns for public outreach will be required. The uplink requirements could include positioning the test cell, focusing the microscope, and varying the heat input and/or heat rejection.

As a minimum, we need to know if the cell is operating properly: sensible temperature profile (to give heat input, heat out in condenser, radiation losses); single bubble in correct location; is the camera focused so that it is recording fringes (pictures of some fringes at the midpoint of the bubble as a function of heat input); calculated curvature at the midpoint of the bubble as a function of the heat input; vapor pressure value; calculated curvature at three other locations to see if there is a curvature gradient.

The minimum subset of downlinked data required to verify proper operation is:

- macroscopic view of test section
- curvature measurements – 3 to 4 values of curvature in 2000 to 20,000 m^{-1} range
- temperature & pressure measurements

5.6 Experiment Data Requirements

The data that will be analyzed needs to be obtained under steady state conditions (at "low heat input rates") or under periodic oscillatory conditions ("higher heat input rates"). The exact range of "low heat input rates" needs to be determined during flight under μg conditions because it is a function of gravity and environmental noise. In a given test with varying heat input rates, steady state data will be obtained first as a function of the heat input rate and until oscillations occur. Then, the test will be continued with the data recorded under oscillatory conditions. The definition of steady state is based on the measured value of the local curvature: i.e., the local value of the curvature associated with the first four destructive interference fringes near the contact line in the middle of the vapor bubble should be steady within the accuracy level given in §5.6.1. The time period of the oscillations are a function of gravity, contact angle, bubble length and the heat input rate.

5.6.1 Curvature Measurements

Figure 9 on page 22 illustrates the theoretical value of the curvature in the corners of a cuvette plotted as a function of the axial position and the axial heat flow rate. The curvature measurements should be sufficient to determine the axial curvature profile for all heat inputs for comparison to the theoretical profile. To that end, the axial and lateral position of the following curvature measurements are required [§]:

- 1000 to 4000 m^{-1} at 200 m^{-1} increments with an absolute value of ± 100 m^{-1}
- 4000 to 20,000 m^{-1} at 1000 m^{-1} increments with an absolute value of ± 500 m^{-1}

[§]The curvature will be determined by the PI using the image data obtained.

The maximum number of curvature measurements for a given heat input will be 36. This maximum number of measurements will occur at the higher heat fluxes (see Figure 9, page 22). For low heat inputs, the higher curvature values may not exist. Therefore, if the entire axial length of the vapor bubble has been measured, then the measurements will be considered complete for that heat input. The axial and lateral position of each curvature measurement relative to the test cell must be known to within ±0.025 mm. The range and accuracy of the curvature measurements must be:

- $600 \leq K \leq 20{,}000\ \mathrm{m}^{-1}$ ±4%

The accuracy of the curvature measurements is specified for pentane as the working fluid. It is recognized that with ethanol as the working fluid, the curvature measurements will not be as accurate as with pentane. However, the accuracy with ethanol will be acceptable provided the accuracy of the curvature measurements is maintained with pentane.

Each curvature measurement should be sampled at a minimum of 30 Hz for at least 3 seconds in order to capture an anticipated 10 Hz oscillation without aliasing. The maximum time between consecutive curvature measurement locations should not exceed 2 minutes.

Current studies at Rensselaer (outlined in §8 Appendices A,B,C,D) use an Image Analyzing Interferometer, IAI, to determine the film thickness profile. Using image processing, the film thickness profile gives the curvature profile and, therefore, the pressure field for liquid flow in the liquid film. From the experiments, we need to know the curvature profile with the accuracy specified above. As a minimum, we need the local value of the curvature associated with the first four destructive interference fringes near the contact line. Based on improvements made in IAI techniques developed in our laboratory, the thickness, slope and curvature profiles will be obtained from the image data. Recent advancements in the technique can be found in Gokhale et al.

5.6.2 Film Thickness Measurements

In addition to measuring the curvature, the adsorbed film thickness and an absolute film thickness are required over the axial length of the vapor bubble. A film thickness measurement is required at a point in the constant curvature portion of the film profile in the same location that the curvature measurement is taken. Likewise, the adsorbed film thickness corresponding to each curvature measurement location is required. Thus, the curvature profile data set should have a corresponding film thickness data set as well as an adsorbed film thickness data set.

The range of film thickness measurements should be from 10 nm to 20 μm with an accuracy of ±10 nm. The location of the film thickness measurement should correspond to the center of the curvature measurement location and be known to within ±0.025 mm. In addition to the film thickness measurement, the adsorbed film thickness must be determined to within ±10 nm at each axial location that the curvature and film thickness measurements are acquired. Figure 10 illustrates the required curvature (K), film thickness (δ), and adsorbed film thickness (δ_o) measurements for

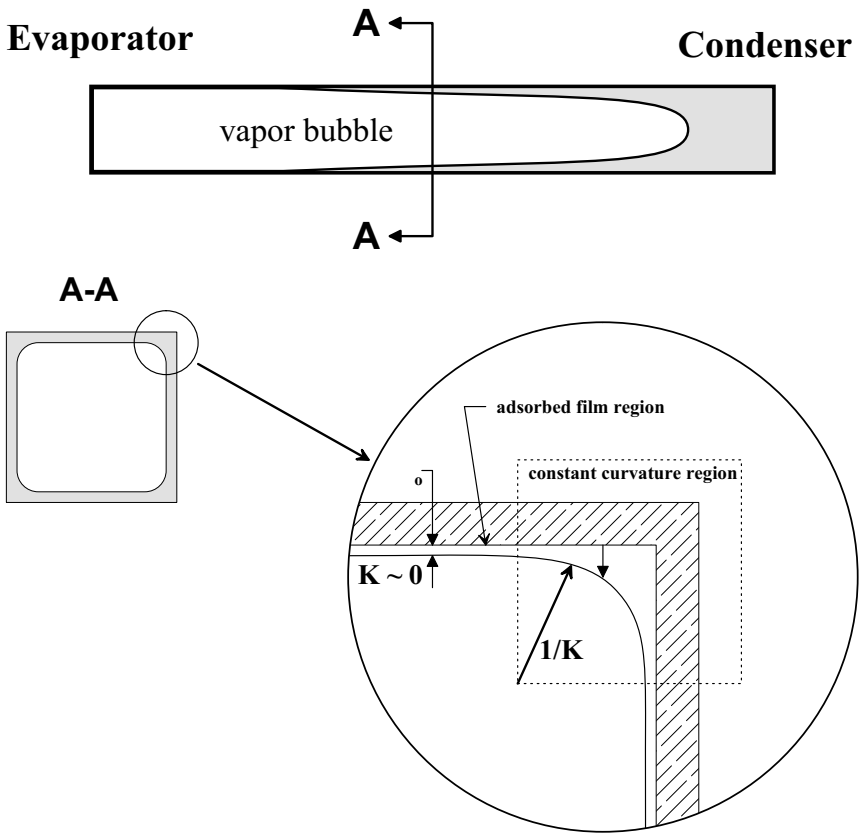

Figure 10. Illustration of the curvature and thin film measurements for a specific axial position.

one axial position of the test section.

Each set film thickness and adsorbed film thickness measurements should be sampled at a minimum of 30 Hz for at least 3 seconds in order to capture an anticipated 10 Hz oscillation without aliasing. The maximum time between consecutive film thickness and adsorbed film thickness measurements locations should not exceed 2 minutes.

The current technique used for calculating the film thickness from the interferometric data is described in the appendices (§8). The capabilities of the current interferometric system are:

Range	10 nm $\rightarrow$ 20 μm
Accuracy	$\pm$10 nm
Field of View	100 – 150 $\pm$5 μm
System	Image Analyzing Interferometer, IAI,
	Images stored in uncompressed TIFF format
Operating Wavelengths	2 wavelengths separated by $\approx$ 100 nm
	One green ($\sim$ 543 nm)

To obtain the adsorbed film thickness profile, we can use the returned raw reflectivity and image data. The technique for determining the adsorbed film thickness is described in Ling Zheng, "Experimental and Theoretical Investigation of the Loop Constrained Vapor Bubble", Ph.D. Dissertation Proposal, Chemical Engineering, Rensselaer Polytechnic Institute, Troy, New York, February 2001.

5.6.3 Vapor Bubble Observations

These requirements specify a set of coarse measurements concerned with the general macroscopic state of the test section; that is, the shape of the vapor bubble, the shape of the dry-out region, and detection of macroscopic anomalies which might disrupt the system.

A macroscopic determination of the shape and location of the vapor bubble is required in order to verify that there is only a single vapor bubble between the evaporator and condenser and to observe the general shape of the dry-out region. This macroscopic data will also be used to evaluate anomalous behavior in the temperature profile data, etc. Therefore, a macroscopic view of the liquid-vapor configuration is required at a minimum of 30 Hz in order to capture an anticipated 10 Hz oscillation with a resolution of no less than 500 μm and a field of view encompassing the test section (evaporator to condenser). This data is critical during periods of translation of either the test cell or the microscope.

The presence of small bubbles or debris ($\sim$100 μm) in the corners of the test cell may result in a severe disruption of the liquid flow into the evaporator section. While it is not possible to predict or prevent the formation of small bubbles or the accumulation of debris, the disruption of the liquid flow should be detected. Potential methods for accomplishing this requirement may include visualization or temperature measurements.

5.6.4 Heat Input/Rejection Measurements

The heat input into the evaporator and the heat rejection at the condenser must be known to within $\pm$10% for all heat input/rejection levels. The frequency of the heat flow data provided should be 1/60 Hz.

5.6.5 Temperature Measurements

As a minimum, the temperature profile is needed to verify heat input, heat rejection to the condenser, and radiation losses. The temperature profile is also needed to verify that the vapor pressure measurement correlates with the temperature in the condensation region, and to verify the mode of operation (steady vs. unsteady). The additional temperature measurements in the corner, etc. will allow us to numerically calculate a three dimensional temperature field and the heat transfer coef-

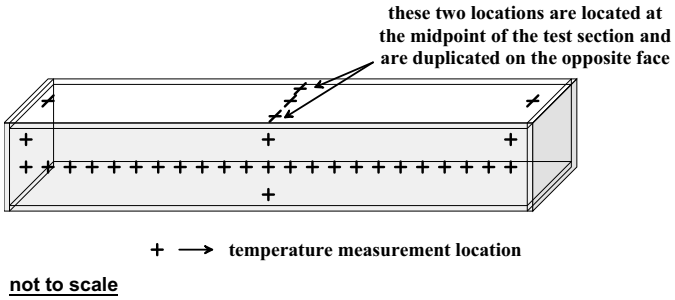

Figure 11. Schematic of temperature measurement locations (not to scale)

ficient inside the test cell. For each heat input, we need to have a three dimensional understanding of the temperature field.

The range of temperatures which may be necessary to measure is from -25 °C to 375 °C at an accuracy of ±0.5 °C. The locations for measuring temperature are illustrated in Figure 11. The locations for which temperatures must be known are:

- test cell face for axial temperature measurements:
  - on centerline of test cell every 1.5 mm from the evaporator to the condenser;
  - one (1) measurement at 1.5 mm from both edges of a corner at the condenser end;
  - one (1) measurement at 1.5 mm from both edges of a corner at the evaporator end;
- orthogonal face:
  - one (1) measurement at 2.0 mm from the condenser end on the centerline;
  - one (1) measurement at 2.0 mm from the evaporator end on the centerline;
  - one (1) measurement at the midpoint of the test section;
  - two (2) measurements at 1.5 mm from opposite edges of the midpoint of the test section;
- face opposite opposite orthogonal face:
  - two (2) measurements at 1.5 mm from opposite edges of the midpoint of the test section;

The locations of the temperature measurements must be within ±0.25 mm of the nominal specified location; however, the locations must be known to within ±0.1 mm in both the axial and lateral direction relative to the test cell. The accuracy of the temperature measurements must be ±0.5 °C and must be measured at a frequency of at least 1/60 Hz.

5.6.6 Pressure Measurements

The pressure measurements are required in order to determine if the test cell has a very slow leak to determine the amount of non-condensables in the system. In addition, the pressure measurement

should correlate with the temperature in the region of condensation. The location is not important because there is only a very small pressure gradient in the vapor space due to its large cross-sectional area.

The pressure should be measured in the liquid on the condenser side of the test cell. The pressure must be measured over the range of 280 to 1000 Torr with an accuracy of ± 5 Torr at a resolution of ± 1 Torr. The pressure must be sampled at a frequency of at least 1/60 Hz.

The pressure measurements can also be used to tell us about the transient change of temperature within the test cell between changes in the heat input. The pressure measurements will also provide information about oscillations in the overall process.

5.6.7 Acceleration Measurements

The residual accelerations of the environment may affect the stability of the evaporating liquid film. The acceleration frequencies of interest are from 0 to 50 Hz with a resolution of at least 100 Hz. The minimum peak acceleration levels of interest are 10^{-6} g's. The absolute values of accelerations above 10^{-3} are not required, but the direction and time of such accelerations must be provided.

In the current design concept for CVB, the test section is translated beneath a stationary microscope in order to acquire each curvature and film thickness measurement. It is critical to measure the acceleration of the test section during these translation. These accelerations are considered to be of 0 frequency relative to the residual accelerations of the environment. The dc acceleration of the test section during experiment operations should be measured at an accuracy of 10^{-5} g's and sampled at 100 Hz.

5.6.8 Correlation of Experiment Data

The required experimental data specified in §5.6 must be correlated to within 1/30 of a second for every test run. This requirement includes data not specifically gathered by the CVB experiment; such as acceleration data.

5.7 Test Matrix and Experiment Operations

It is anticipated that there will be two primary modes of operation for the CVB test cell; steady and unsteady. The unsteady operation will be characterized by oscillations of the thin film profile. Steady state operation is achieved when the average curvature at a given axial position (e.g., midplane of the bubble) does not change by more than $\pm 5\%$ when $K < 20{,}000$ over a period of 10 minutes. For steady operation of the dry cell, see the discussion of tracking temperature in §5.5.2.

The CVB test matrix, summarized in Table 2, is designed to achieve the following:

1. Find the external heat transfer coefficient from the temperature data of the dry cell for the purpose of calibrating the system.
2. Measure the equilibrium film thickness and curvature profiles, and compare these measurements with the Augmented Young-Laplace equation.
3. Check the extended meniscus profile in microgravity and compare it with ground based measurements.
4. Determine the effect of the heat input and heat rejection on the shape and location of the vapor bubble.
5. Determine the time duration for the test cell to reach thermal equilibrium and measure the equilibrium temperature profile.
6. Measure the temperature profile, film thickness profile and curvature profile (both along the cell axis and transverse to the cell axis) as a function of heat input and/or rejection.
7. Measure the vapor pressure and compare with the operating temperature measurements.
8. Calculate the amount of fluid which can be pumped along the corners in a microgravity environment.
9. Determine the maximum heat load before dryout occurs at the hot end, the shape of the dryout region, and the effect of the fill ratio on the maximum heat load.
10. Calculate the thermal conduction in the glass vs. the effective thermal conductance of the evaporation/condensation process in the test cell.
11. Determine the onset, mode and mechanism of cavitation and/or instability of the thin liquid film.
12. In general, determine where and how does a low capillary pressure CVB with $(\sigma \mathrm{K} + \Pi) > 0$ become unstable.

Table 2: Synopsis of CVB Test Matrix

Test	**Substrate**	**Bubble Length**	**Heat In/Out**
1	Quartz Vacuum	Dry Cell	Start with 0 W and increase in 0.01 W increments until temperature of the heater reaches 350 °C. Afterwards decrease in 0.01 W increments back to 0 W.
2	Quartz Pentane	40 mm a. (Low mag 10x recommended) b. (High mag 50x recommended)	Start with 0 W and increase in 0.2 W increments up to 0.6 W. This is followed by an increase from 0.8 W (including data at 0.8 W) to 2.0 W in 0.4 W increments. Image data of the **entire bubble** is taken with low magnification objective. Afterwards decrease using 0.4 W increments to 0.8 W followed by decrements of 0.2 W to 0 W With the data collected using the Low magnification objective, six (6) positions would be chosen for study with a high magnification. Same power settings will be used.
3	Quartz Pentane	30 mm	Same as Test 2.
4	Quartz Ethanol	25 mm ¶	Same as Test 2.
5	Quartz Pentane	20 mm	Same as Test 2.

¶The size of the bubble and putity of the ethanol is being reevaluated

Initial Questions to be Addressed by the CVB Experiment

1. How effective is radiative cooling?
2. How do the size, shape and location of the vapor bubble change as a function of power input and removal?
3. Is a single bubble stable in microgravity while evaporation/condensation is occurring? For which fill ratios?
4. Can bubble location be manipulated easily by varying the temperature? For which fill ratios?
5. How long does it take to establish macroscopic mechanical equilibrium when a transport process is occurring?
6. How long does it take to establish thermal equilibrium?
7. Does dry out occur? What is the shape of the dry area?
8. What is the phenomena causing instability? What is the effect of capillary pressure level on the onset of instability, i.e. the axial location?
9. What is the value of the maximum axial heat flux?
10. Does the CVB function better as a heat pipe in microgravity as compared to the earth's gravity environment?
11. What are the macroscopic transport characteristics of the CVB test cell?

Additional Questions on Details of the CVB Operation

1. How does vapor bubble location, shape and size vary with the overall pressure and temperature difference?
2. How does the film thickness profile and curvature profile vary axially and radially in the cell for each power input?
3. How much fluid can be pumped along the corners in a microgravity environment? What is the maximum heat load before dryout? When does conduction in the glass outweigh evaporation/condensation in the cell?
4. Can the system work as a reliable heat transfer device in microgravity? For which heat loads? What is the value of the thermal conductance?
5. Is there a significant difference in maximum heat load for the different bubble lengths in microgravity?

6. Can we predict the bubble size, shape, and heat duty of the device in microgravity? Can we predict maximum performance, dryout area shape, and stability?
7. Do instabilities and oscillations in film thickness occur at the same power inputs in a microgravity environment?
8. Do instabilities and oscillations in film thickness and/or cavitation occur at the same heat flux distribution (or film thickness, pressure gradient, capillary pressure) for each fill?
9. Do instabilities disappear at the same power level when the power is reduced, i.e. hysteresis effects?
10. How well does the Kelvin-Clapeyron model predict heat fluxes?

5.7.1 Dry Cell Operations

1. Verify proper environmental conditions before starting test (§5.4.3 and §5.4.4).
2. Check pressure to insure test cell has not leaked.
3. Turn on heater (0 W) and step up power input in (0.01 W) increments until the heater temperature reaches 350 °C. Temperature and "pressure" measurements should be made at each power setting. Record the time to steady-state.
4. Operate the test cell in the reverse manner starting at the highest power level and decreasing in appropriate increments.

5.7.2 Wet Cells Operations

1. Verify proper environmental conditions before starting test (§5.4).
2. Record the initial location, size and shape of the vapor bubble. Record the equilibrium adsorbed film thicknesses. Record the curvature, film thickness, and temperature profiles. Record the pressure and acceleration measurements.
3. Turn on heater (0 W) and observe location, size and shape of the vapor bubble. This consists of the isothermal reading.
4. Set the cooler to a constant value (15 °C is recommended).
5. Collect data using a low magnification objective (10x recommended). If the heat input is less than the maximum as defined in §5.5.1 and if the system is steady enough to collect meaningful data, then:
   (a) Record location, size, and shape of vapor bubble.
   (b) Record the corner meniscus image at low magnification.

(c) Record the temperature, pressure, heat input/rejection, and acceleration measurements.

(d) Record the time to steady-state and the shape of the dry area.

(e) Record location and occurrence (heat input, ΔT, and P) of any instabilities (oscillations) in the film thickness profile.

6. Increase the heat input by the appropriate increment (see §5.7) and repeat Step 5.

7. Repeat Steps 5 and 6 starting from the highest heat inputs and decreasing in suitable increments as given in §5.7 to 0 W. Note any hysteresis effects at the heat inputs associated with the onset or decay of instabilities in the film thickness profile because of changes in the interfacial force field resulting from "aging" of the substrate and fluid.

8. Choose six (6) locations from the low magnification data where data at high magnification should be collected. This can be done by the PI.

9. With a high magnification objective (50x recommended) and using the positions determined in Step 8, repeat from Step 1 to 7 for the heat flux settings in §5.7.

5.8 Success Criteria

Prior to the pre-ship review, this section will be revised as details of the CVB experiment hardware capabilities and the capabilities of the microgravity facilities (Light Microscopy Module (LMM), Fluid Integrated Rack (FIR), and International Space Station (ISS)) become better defined. A summary of the minimum and comprehensive success criteria is given in Table 3.

5.8.1 Criteria for Minimum Success

1. Fly five (5) CVB cells including the dry cell per specifications in §5.4.1.

2. For the dry cell, record temperature profile for three (3) values of heat flux.

3. For three (3) values of the fill ratio (2 pentane and 1 ethanol) and three (3) values of the heat flux at each fill ratio, record the following:

   (a) measurement of the size of the dry area, size and shape of the region of evaporation, and the stability of the evaporating thin film;

   (b) measurement of the curvature profiles in the intermediate region;

   (c) measurement of the heat input, heat rejection, pressure, and temperature profile; and

   (d) obtain general observations concerning the operation of the cell under nonisothermal conditions (e.g., do oscillations occur in the location of the contact line? What are the effects of oscillations and cavitation on stability?).

   If one of the pentane test cells is lost, twelve (12) values of the heat flux with one of the other fill ratios will give minimum success because the regions can overlap.

4. Record and time correlate all the above data and transfer to the Principal Investigator.

5.8.2 Criteria for Comprehensive Success

1. Completion of Minimum Success Criteria (§5.8.1).
2. For all values of the fill ratio and six (6) values of the heat input for each fill ratio, record the following:
   (a) all measurements described in the criteria for minimum success;
   (b) measurements of film thickness profiles at a minimum of four (4) axial positions in the intermediate section and four (4) positions in the evaporator section;
   (c) measurement of the adsorbed film thicknesses; and test cell;
   (d) measurement of accelerations.
3. Observation of dryout and thickness instabilities for at least one value of heat input for each wet test cell.
4. Record and time correlate all the above data and transfer to the Principal Investigator.

5.9 Post Flight Deliverables To the Principal Investigator

For each test run the following deliverables will be supplied to the Principal Investigator for post-flight analysis.

1. Time correlated equilibrium data:
   (a) film thickness and curvature profiles;
   (b) vapor bubble observations;
   (c) heat input and heat rejection to cooler;
   (d) all temperature measurements on test cell; and
   (e) pressure and accelerations measurements.
2. Time correlated non-equilibrium data:
   (a) curvature profiles, film thickness profiles, and adsorbed film thicknesses;
   (b) vapor bubble observations;
   (c) heat input and heat rejection to cooler;
   (d) all temperature measurements on test cell; and
   (e) pressure and accelerations measurements.
3. All CVB flight cells for post-flight analysis.

Table 3. Summary of CVB Success Criteria

		success criteria	
parameter	**section**	**minimum**	**comprehensive**
fill ratio	§5.4.1	3	all
heat input per fill ratio	§5.5.1	3	6
curvature profile	§5.6.1	√	
film thickness profile & adsorbed film thickness	§5.6.2		√
vapor bubble observations	§5.6.3	√	
heat input/rejection	§5.5.1 & §5.5.2	√	
temperature profile	§5.6.5	√	
pressure	§5.6.6	√	
acceleration	§5.6.7		√
unsteady operation mode	§5.8.2		√
delivery of time correlated data	§5.6.8	√	√

NOTE: Time correlated, uncompressed TIFF images of the dual-wavelength interferometric fringe patterns and gray values may be provided to the Principal Investigator for post processing instead of items 1a and 2a listed above. The fringe patterns must be of the quality and frequency to meet the requirements for curvature, film thickness, and adsorbed film thickness data as specified in §5.6.1 and §5.6.2.

5.10 Conclusions

- Based on viscous losses in the corners, the maximum attainable axial heat flow rate increases with the cube of the characteristic width of the non-equilibrium CVB.
- Based on viscous losses in the corners, the maximum attainable axial heat flux increases linearly with the characteristic width of the CVB.
- Low capillary pressure systems (relatively large widths) are desirable heat transfer systems.
- Microgravity allows the axisymmetric study of a larger range of low capillary pressure systems, which have large characteristic widths.
- The effects of stability, oscillations, and cavitation in the thin film region on the maximum attainable heat flux is unknown.
- To enhance the understanding of passive, change-of-phase, high heat flux, low capillary pressure systems, the CVB should be studied under microgravity conditions.
- Therefore, extensions of our current studies of the non-equilibrium CVB to a microgravity environment are proposed to obtain "**axisymmetric**" profiles under low Bond number conditions which will give a more definitive understanding of high flux, passive, change-of-phase systems.

6 References

Babin, B. R., Peterson, G.P., and Wu, D., 1990, "Steady State Modeling and Testing of a Micro Heat Pipe," *ASME J. of Heat Transfer*, **112**, pp. 595-601.

Blake, T. D., 1975, "Investigation of Equilibrium Wetting Films of n-alkanes on a-alumina", *J. Chem. Soc., Faraday Trans. 1*, **71**, p. 192.

Brown, J. R., Chang, W. S., Halliman, K. P., and Chebaro, H. C., "Heat Transfer from Stable Evaporating Thin Films in the Neighborhood of a Contact Line", 1993, 93-HT-4, *Proc. of National Heat Transfer Conf.*, Atlanta, GA.

Concus, P, 1968, "Static Menisci in a Vertical Right Circular Cylinder", *J. Fluid Mechanics*, **34**, pp. 481-495.

Cotter, T. P., 1984, "Principles and Prospects of Micro heat Pipes", Proc. 5th Int. Heat Pipe Conf., Tsukuba, Japan, pp. 328-335.

DasGupta, S., Plawsky, J. L., and Wayner, P. C., Jr., 1995, "Interfacial Force Field Characterization in a Constrained Vapor Bubble Thermosyphon", *AIChE Journal*, **41**, pp 2140-2149. Included in SRD as Appendix A.

DasGupta, S., Schonberg, J. A., Kim., I., Y., and Wayner, P. C. Jr., 1993a, "Use of the Augmented Young-Laplace Equation to Model Equilibrium and Evaporating Extended Menisci", *J. Colloid Interface Sci.*, **157**, p. 332.

DasGupta, S., Schonberg, J. A., and Wayner, P. C., Jr., 1993b, "Investigation of an Evaporating Extended Meniscus Based on the Augmented Young-Laplace Equation", *J. Heat Transfer*, **115**, p. 201.

DasGupta, S., Sujanani, M., and Wayner, P.C., Jr., 1991, "Microcomputer Enhanced Optical Investigation of an Evaporating Liquid Film Controlled by a Capillary Feeder", *Proc. of the 2nd World Conf. on Experimental Heat Transfer, Fluid Mechanics & Thermodynamics*, Keffer, J. F. et al. ed., Elsevier, New York, p. 361.

DasGupta, S., Kim, I. Y., and Wayner, P. C., Jr., 1994, "Use of the Kelvin-Clapeyron Equation to Model an Evaporating Curved Microfilm", *J. Heat Transfer*, **116**, pp. 1007-1015.

de Feijter, J. A., 1988, "Thermodynamics of Thin Films", *Thin Liquid Films, Fundamentals and Applications*, edited by I. B. Ivanov, 1st edition, Marcel Dekker, New York, NY, pp. 1-47.

deGennes, P. G., 1985, "Wetting: statics and dynamics", *Reviews of Modern Physics*, **57**, p. 289.

Derjaguin B. V., and Kussakov, 1939, *Acta Physicochim URSS*, **10**, p. 25.

Derjaguin, B. V., Nerpin, S. V., and Churaev, N. V., 1965, "Effect of Film Transfer upon Evaporation of Liquids from Capillaries", *Bulletin Rilem*, No. 29, p. 93.

Derjaguin, B.V., and Churaev, N.V., 1976., "The Definition of Disjoining Pressure and its Importance in the Equilibrium and Flow of Thin films", *Colloid J. USSR*, **38**, p. 438.

Dzyaloshinskii, I. E., Lifshitz, E. M., and Pitaevskii, L. P., 1961, "The General Theory of van der Waals Forces', *Ad. Phys.*, **10**, p. 165.

Faghri, A., 1995, "Heat Pipe Science and Technology", First Edition, Taylor and Francis, Washington, DC.

Gokhale, S. J., DasGupta S., Plawsky, J. L., and Wayner, P.C., Jr., 2004, "Reflectivity-based evaluation of the coalescence of two condensing drops and shape evolution of the coalesced drop", *Phy. Rev. E*, **70**, p. 051610

Ha, J. M. and Peterson, G. P., 1998, "Capillary Performance of Evaporating Flow in Micro Grooves: An Aalytical Approach for Very Small Telt Angles", *J. Heat Transfer*, **120**, pp. 452-457.

Hirasaki, G. J., 1990, in "Interfacial Phenomena in Petroleum Recovery", N. R. Morrow, Ed., Dekker, New York.

Holm, F. W., and Goplen, S. P., 1979, "Heat Transfer in the Meniscus Thin-Film Transition Region", *J. Heat Transfer*, **101**, p. 543.

Huang, J., Karthikeyan, M., Plawsky, J., and Wayner, P. C., Jr., 1998, Experimental Study and Modeling of the Effect of Low-level Impurities on the Operation of the Constrained Vapor Bubble", STAIF-98, Part I, pp 446-451, Albuquerque, NM, Jan. 25-29.

Huh, C. and Scriven, L.E., 1971, Hydrodynamic Model of Steady Movement of a Solid/Liquid/Fluid Contact Line, *J. Colloids Interface Science*, **35**, p. 85.

Kamotani, Y., 1978, "Evaporator Film Coefficients of Grooved Heat Pipes", *Proc. 3rd Int. Heat Pipe Conf.*, Palo Alto, CA.

Khrustalev, D., and Faghri, A., 1993, "Thermal Analysis of a Micro Heat Pipe", *Proc. of National Heat Transfer Conf.*, Atlanta, GA.

Kim, I-Y, and Wayner, P.C., Jr., 1996, "Shape of an Evaporating Completely Wetting Extended Meniscus", *J. Thermophysics and Heat Transfer*, **10** (2), p. 320.

Lam, A.C., and Schechter, R.S., 1991, "A Note on the Transition Region Connecting Thin to Thick Films", *J. Colloids Interface Science*, **146**, p. 206.

Longtin, J. P., Badran, B., and Gerner, F. M., 1994, "A One-Dimensional Model of a Micro Heat Pipe During Steady State Operation", *ASME J of Heat Transfer*, **116**, pp. 709-715.

Martynov, G. A., Starov, V. M., and Churaev, N. V., 1977, "Hysteresis of the Contact Angle at Homogeneous Surfaces", *Kolloidnyi Zhurnal* (English Translation), **39**, pp. 406-417.

Moosman, S. and Homsy, S.M., 1980, "Evaporating Menisci of Wetting Fluids", *J. of Colloid & Interface Sci.*, **73**, p. 212.

Peterson, G. P., 1992), "Overview of Micro Heat Pipe Research and Developments", *Appl. Mech. Rev., ASME*, **45** (5), p. 175.

Potash, M., Jr. and Wayner, P.C., Jr., 1972., "Evaporation from a Two-Dimensional Extended Meniscus", *Int. J. Heat Mass Transfer*, **15**, p. 1851.

Renk, F., Wayner, P.C., Jr., and Homsy, G.M., 1978, "On the Transition between a Wetting Film and a Capillary Meniscus," *J. Colloid and Interface Sci.*, **67**, p. 408.

Stephan, P. C. and Busse, C. A., 1992, "Analysis of the Heat Transfer Coefficient of Grooved Heat Pipe Evaporator Walls", *Int. J. Heat Mass Transfer*, **35**, pp. 383-391.

Swanson, L. W., and Herdt, G. C., 1992, "Model of the Evaporating Meniscus in a Capillary Tube", *J. Heat Transfer*, **114**, p. 434.

Swanson, L. W., and Peterson, G. P., 1993, "The Interfacial Thermodynamics of the Capillary Structures in Micro Heat Pipes", *Proc. of National Heat Transfer Conf.*, Aug. 8-11, Atlanta, GA .

Takamatsu, H., Fujii, M., and Honda, H., 1996, Behavior of an Air-Water Interface in a Horizontal Closed Pipe Suddenly put under Micro-Gravity Condition, HTD Vol. 324, *National Heat Transfer Conference*, **2**, ASME, NY, NY.

Teletzke, G. F., Scriven, L. E., and Davis, H. T., 1987, "How Liquids Spread on Solids", *Chem. Eng. Comm.*, **55**, p. 41.

Truong, J.G. and Wayner, Jr., P.C., 1987, "Effect of Capillary and Van der Waals Dispersion Forces on the Equilibrium Profile of a wetting Liquid: Theory and Experiment", *J. Chem. Phys.*, **87**, 4180.

Wayner, P.C., Jr., 1979, "Effect of Thin Film Heat Transfer on Meniscus Profile and Capillary Pressure", *AIAA Journal*, **17**, pp. 772-776.

Wayner, P.C., Jr., Kao, Y.K., and LaCroix, L.V., 1976, "The Interline Heat Transfer Coefficient of an Evaporating Wetting Film", *Int. J. Heat Mass Transfer*, **19**, p. 487.

Wayner, Jr., P.C., 1991, "The Effect of Interfacial Mass Transport on Flow in Thin Liquid Films", *Coll. and Surfaces*, **52**, p. 71.

Wong, H., Morris, S., and Radke, C. J., 1992, *J. Colloid and Interface Science*, **148**, pp 317-336.

Wu, D. and Peterson, G. P., 1991, "Investigation of the Transient Characteristics of a Micro Heat Pipe", *J. Thermophysics*, **5**, p. 129.

7 Nomenclature

$\bar{A}$	=	$A/(6\pi)$
a	=	See Figure 4
C	=	Corner shape factor
g	=	gravitational force per unit mass
H	=	See Figure 4
h	=	enthalpy/mass or volume
K	=	curvature
k	=	friction factor coefficient
L	=	flow length
Q	=	axial heat flow rate
q	=	heat flux
V	=	velocity
x	=	axial position
z	=	axis
D	=	dimensionless thickness
d	=	liquid film thickness
q	=	local angle of l-v interface
m	=	viscosity
P	=	disjoining pressure
s	=	surface free energy per unit area
t	=	shear stress
r	=	fluid density
n	=	kinematic viscosity

Subscripts and Superscripts

c	=	condenser
fl	=	friction in liquid
fg	=	heat of vaporization
l	=	liquid
o	=	reference or equilibrium film thickness of flat film
s	=	solid
v	=	vapor
μ	=	microgravity
‘	=	derivative
∞	=	reference

8 Titles of Attachments

ATTACHED APPENDIX A: "Interfacial Force Field Characterization in a Constrained Vapor Bubble Thermosyphon"

ATTACHED APPENDIX B: "Experimental Study and Modeling of the Intermediate Section of the Non-isothermal Constrained Vapor Bubble"
APPENDIX B2: "Constrained Vapor Bubble" additional data presented at 1998 International Heat Transfer Conference

ATTACHED APPENDIX C: "Experimental Study and Modeling of the Effect of low-Level Impurities on the Operation of the Constrained Vapor Bubble"

ATTACHED APPENDIX D: "Use of the Kelvin-Clapeyron Equation to Model an Evaporating Curved Microfilm'